

Mosaic3D: Foundation Dataset and Model for Open-Vocabulary 3D Segmentation

Junha Lee^{1,2,†} Chunghyun Park^{1,2,†} Jaesung Choe¹
 Yu-Chiang Frank Wang¹ Jan Kautz¹ Minsu Cho² Chris Choy¹

¹NVIDIA ²POSTECH



Figure 1. **Mosaic3D-5.6M.** Mosaic3D-5.6M is a large-scale dataset generated from a collection of existing datasets [7, 14, 24, 99, 107], consisting of 5.6M mask-text pairs, providing fine-grained masks (black outline in the figure) and detailed captions (text with matching color) pairs. Using this large-scale dataset, we propose Mosaic3D, a foundation model for open-vocabulary 3D segmentation.

Abstract

We tackle open-vocabulary 3D scene segmentation tasks by introducing a novel data generation pipeline and training framework. Our work targets three essential aspects required for an effective dataset: precise 3D region segmentation, comprehensive textual descriptions, and sufficient dataset scale. By leveraging state-of-the-art open-vocabulary image segmentation models and region-aware vision-language models (VLM), we develop an automatic pipeline capable of producing high-quality 3D mask-text pairs. Applying this pipeline to multiple 3D scene datasets, we create Mosaic3D-5.6M, a dataset of more than 30K annotated scenes with 5.6M mask-text pairs - significantly larger than existing datasets. Building on these data, we propose Mosaic3D, a 3D visual foundation model (3D-VFM) combining a 3D encoder trained with contrastive learning and a lightweight mask decoder for open-vocabulary 3D semantic and instance segmentation. Our approach achieves state-of-the-art results on open-vocabulary 3D semantic and instance segmentation benchmarks including ScanNet200, Matterport3D, and ScanNet++, with ablation studies validating the effectiveness of our large-scale training data. <https://nvlabs.github.io/Mosaic3D/>

1. Introduction

3D scene understanding is a fundamental problem in computer vision that involves detecting and localizing objects while comprehending complex spatial relationships in 3D environments. This capability is essential for various applications, including robotics, AR/VR, human-computer interactions, and autonomous vehicles. While traditional approaches rely on predefined object categories, the field is evolving toward open-vocabulary 3D scene understanding, where systems can recognize arbitrary concepts without being constrained to the predefined label sets. Despite humans’ innate ability to perform such tasks effortlessly, developing comparable machine capabilities remains an open problem.

The key bottleneck in advancing open-vocabulary 3D scene understanding is the scarcity of large-scale, high-quality training data. This limitation is particularly striking compared to 2D vision-language models [31, 34, 38, 51, 53–56, 71, 73, 83, 96, 104], which have achieved remarkable open-vocabulary capabilities through training on web-scale image-text pair datasets [11, 16, 30, 71, 81]. Unfortunately, creating datasets of comparable scale for 3D scenes remains prohibitively expensive and time-consuming.

Training effective open-vocabulary 3D scene understanding models requires datasets that satisfy three critical requirements: (1) precise 3D region annotations that delineate object boundaries, (2) rich textual captions that characterize

[†] Authors equally contributed to this work during internship at NVIDIA.

the visual and semantic attributes of each region, and (3) substantial scale to encompass diverse domains and offer rich visual-semantic variations. Creating such data manually, however, becomes increasingly intractable as datasets grow.

To address these challenges, recent works [27, 48, 98] leverage 2D visual foundation models (VFM) [1, 58, 69, 110] to automate data annotation. They generate 3D mask-text pairs on multi-view RGB-D frames using 2D VFMs and aggregate the generated captions in 3D space. However, they fall short in meeting aforementioned requirements: they use coarse bounding box detectors [27, 98]; only have simple attribute labels [48]; and are limited in scale, containing only a few thousand scenes, as shown in Fig. 4. Existing 3D-text pair datasets for 3D vision-language models [44, 60, 94] also face limitations in both the richness of textual captions and the precision of 3D masks, primarily because they rely on human-annotated object labels and 3D region annotations.

In this paper, we address these limitations by introducing an improved data generation pipeline to create high-quality, large-scale 3D mask-text pairs. Our pipeline satisfies all three criteria by leveraging state-of-the-art open-vocabulary image segmentation models [50, 59, 75, 110] for precise region segmentation and advanced region-aware vision-language models [103] for generating comprehensive textual captions at scale. By applying this pipeline to a diverse collection of 3D scene datasets [7, 14, 24, 99, 107], we create **Mosaic3D-5.6M**, a large dataset containing over 30K scenes with 5.6M region captions – significantly exceeding existing datasets [48, 98] in scale – while maintaining high-quality region masks and detailed textual captions.

Building upon this new dataset, we analyze how improving the annotation quality and scaling up the data impact open-vocabulary 3D scene segmentation. To enable this analysis, we develop a general framework for open-vocabulary 3D semantic and instance segmentation. We train our foundational 3D encoder, **Mosaic3D**, which aligns a per-point feature with a text embedding vector through contrastive learning. Then, we train a lightweight mask decoder to predict object instances directly from language-aligned features, enabling the first single-stage open-vocabulary 3D instance segmentation without ground truth labels. Our approach achieves state-of-the-art results on multiple semantic and instance segmentation benchmarks. Extensive ablation studies show that both the scale and the quality of our dataset are crucial factors that contribute to the superior performance of our approach.

2. Related Work

2D visual foundation models. In recent years, we have witnessed the emergence of large pretrained models—so-called foundation models that are trained on large-scale datasets and serve as a *foundation* for many downstream tasks. These models demonstrate remarkable versatility

across multiple modalities, including language [2, 5, 10, 19, 22, 28, 46, 47, 70, 88, 90, 91, 97], vision [13, 37, 50, 66, 67, 75, 77, 85, 86, 110], audio [8, 26, 79, 105]. Furthermore, they enable multi-modal reasoning capabilities that bridge across different modalities [6, 32, 45, 58, 71, 89]. Among these models, those that operate on visual modalities are known as visual foundation models (VFM). VFMs excel in various computer vision tasks such as image segmentation [17, 18, 43, 50, 52, 75, 109, 110], object detection [12, 59], representation learning [13, 67], and open-vocabulary understanding [20, 31, 41, 49, 51, 63, 71, 102, 106]. When integrated with large language models, they enable sophisticated visual reasoning and natural language interactions [6, 32, 35, 58, 89, 101, 103]. We use such vision language models to construct open vocabulary segmentation and captions for point clouds based on multiview images.

Open-vocabulary 3D segmentation. Building on the success of 2D VFMs, recent work have extended open-vocabulary capabilities to 3D scene understanding. OpenScene [68] first introduced zero-shot 3D semantic segmentation by distilling knowledge from language-aligned image encoders [31, 51]. Subsequent methods [27, 48, 98] leverage multiview images to generate textual captions, which then serve as training supervision. However, these methods face challenges in generating high-quality 3D mask-text pairs at scale. For open-vocabulary 3D instance segmentation, existing methods [42, 65, 87] typically rely on closed-vocabulary proposal networks such as Mask3D [82], which inherently constrains their ability to detect novel object categories. Moreover, these methods leverage 2D VFMs like CLIP [71] for region classification by projecting 3D regions onto multiple 2D views. This approach requires both 2D images and 3D point clouds during inference. Additionally, it necessitates multiple inferences of large 2D models on projected masks, resulting in high computational costs. We address these limitations by developing the first single-stage open-vocabulary 3D instance segmentation model that operates directly in 3D without ground truth labels, using our Mosaic3D-5.6M dataset and Segment3D [40] proposals.

3D vision-language datasets. Several datasets align 3D scenes with textual annotations to facilitate language-driven 3D understanding. ScanRefer [15], ReferIt3D [3] and EmbodiedScan [94] provide fine-grained object-level localization through detailed referential phrases, while ScanQA [4] targets spatially grounded question-answering. In contrast, SceneVerse [44] and MMScan [60] employ large-language models or vision-language models to partially automate annotation. Despite leveraging advanced models, these datasets depend significantly on costly human annotations derived from closed-vocabulary sources, limiting their support for open-vocabulary and scalability for large-scale 3D segmentation tasks.

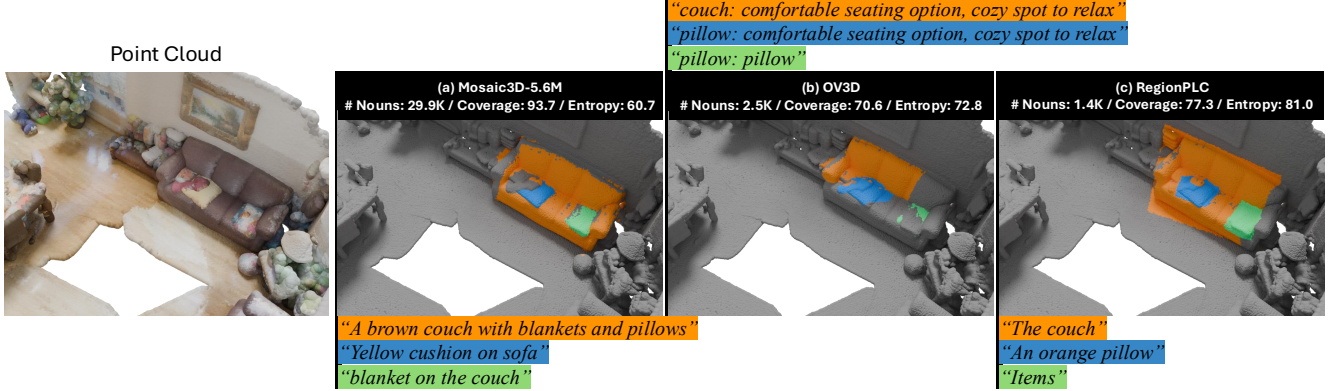


Figure 2. **Dataset comparison.** We compare datasets using three metrics: *# Nouns* (the total number of unique normalized nouns in captions; higher is better), *Coverage* (the percentage of 3D points with associated captions per scene; higher is better), and *Entropy* (the entropy of GT instance ID distribution within masks; lower means more homogeneity - hence better). (a) Mosaic3D-5.6M uses precise masks (Entropy: 60.7) with region-aware VLMs for detailed descriptions (# Nouns: 29.9K). (b) OV3D [48] produces simple attribute labels (# Nouns: 2.5K) lacking comprehensive visual descriptions. (c) RegionPLC [98] uses coarse bounding boxes, yielding imprecise masks (Entropy: 81.0).

3. Mosaic3D-5.6M Data Engine

Generating 3D mask-text pair datasets can be costly and require meticulous attention. Recent work [27, 48, 98] have leveraged 2D visual foundation models (VLMs) to automate data annotation to an extent – they use multi-view images to generate captions or features on different types of region proposals (e.g. bounding boxes, segmentations, or sliding windows). However, existing approaches suffer from imprecise boundary delineation due to their reliance on coarse object detectors [27, 98], or provide only simple attribute labels [48]. To overcome these limitations, we propose a data generation pipeline that combines recent advances in open-vocabulary segmentation and robust region-aware vision-language models (VLMs), enabling both precise region boundaries and rich descriptions that capture object attributes, spatial relationships, and scene context.

3.1. Proposed Pipeline

Our pipeline overcomes limitations through two key improvements: accurate segmentation and the region captioning pipeline. Fig. 3 illustrates the overview of our pipeline. **Enhanced segmentation.** We employ Grounded-SAM [76] and SEEM [110] for more precise open-vocabulary image segmentation. We incorporate both models because Grounded-SAM excels at segmenting foreground objects with precise boundaries, while SEEM complements this with open-vocabulary panoptic segmentation that better handles background stuff like wall and floor. Thus, our method outperforms previous methods [27, 98] that rely on foreground object detectors.

Given an RGB image $\mathbf{I} \in \mathbb{R}^{H \times W \times 3}$, Grounded-SAM first predicts open-set bounding boxes using Grounding-DINO [59], then uses these boxes as input prompts for SAM [50, 75] to generate segmentation masks. To fully au-

tomate the segmentation process, we employ RAM++ [41] to detect object categories within the input image. These detected categories serve as a text prompt for Grounding-DINO. Through this, Grounded-SAM generates a set of segmentation masks $\{\mathbf{M}_k\}_{k=1}^K$ where K is the number of detected objects in the image. Each mask $\mathbf{M}_k \in \{0, 1\}^{H \times W}$ represents a binary segmentation of an object. SEEM operates in a similar way, except that it directly performs panoptic segmentation without being required to use RAM++ to generate tags or Grounding-DINO for object detection. For simplicity, we denote the combined set of masks from both Grounded-SAM and SEEM as $\{\mathbf{M}_k\}_{k=1}^K$, where K is the total number of masks from both models.

Enhanced region captioning. For each segmentation mask, we generate a detailed caption that describes the visual characteristics and spatial context of the object. Unlike previous methods that process an image as a whole using generic image captioning models [1, 58, 69, 93], we leverage region-aware vision-language models (VLMs) [74, 101, 103] that are specifically designed to understand and describe a region or a mask specified by a user as an additional. These models can generate detailed descriptions by interpreting various visual prompts, such as points, boxes, masks, and scribbles, enabling more focused and contextual captions for each segmented region.

Given an image \mathbf{I} , a segmentation mask \mathbf{M}_k , and a user prompt π that asks for a detailed description of the masked region, the region-aware VLM $\mathcal{R}(\cdot)$ generates a textual response c for each mask by $c_k = \mathcal{R}(\mathbf{I}; \mathbf{M}_k, \pi)$, where c_k is a natural language description that captures the visual attributes and spatial context of the k -th masked region. After evaluating several available region-aware VLMs, we chose Osprey [103] for our implementation.

2D pixel-3D point association. After obtaining segmenta-

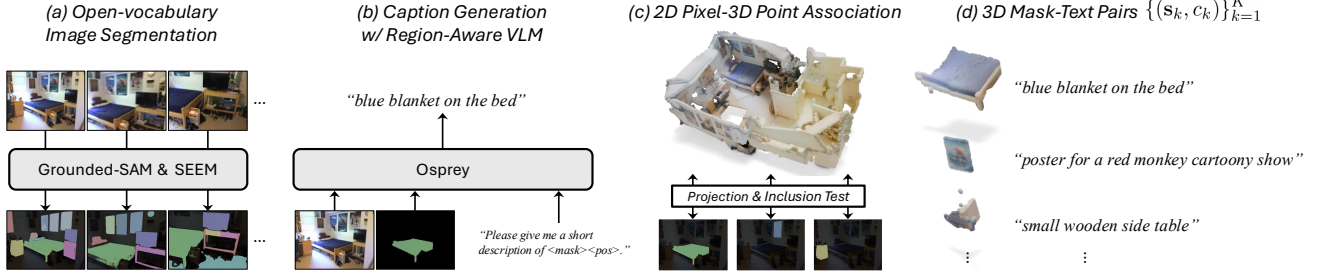


Figure 3. **Mosaic3D-5.6M data engine.** Our data generation process consists of three key steps: (a) We predict object segments for each RGB frame using state-of-the-art image segmentation models [50, 75, 110]. (b) We pass the images and predicted masks to a region-aware vision-language model [103] to generate descriptive captions for each region. (c) We project the 2D segmentation masks onto 3D points using camera parameters to create (d) 3D mask-text pairs. This pipeline enables us to generate a large-scale dataset of 3D mask-text pairs.

tion masks and captions from multiple views, we associate them with 3D points to create mask-text pairs in 3D space. For each 3D point \mathbf{p} in the point cloud $\mathbf{P} \in \mathbb{R}^{N \times 3}$, we project it onto each view using the camera parameters to obtain its 2D pixel coordinates (u, v) and depth value d . We check if the projected pixel falls within any segmentation mask \mathbf{M}_k and if its depth matches the ground-truth depth at that location within a small threshold ϵ (inclusion test). Specifically, for point cloud \mathbf{P} , we compute 3D binary region masks $\mathbf{s}_k \in \{0, 1\}^N$ as:

$$\mathbf{s}_k = \begin{cases} 1 & \text{if } (\mathbf{M}_k)_{u,v} = 1 \text{ and } |d - \mathbf{D}_{u,v}| < \epsilon \\ 0 & \text{otherwise} \end{cases}, \quad (1)$$

where \mathbf{D} is the ground-truth depth image. Finally, we obtain 3D mask-text pairs $\{(\mathbf{s}_k, c_k)\}_{k=1}^K$ that associate each segmented region with its corresponding caption.

Our pipeline produces high-quality 3D mask-text pairs that combine precise object boundaries with rich semantic descriptions. As demonstrated in Fig. 2, compared to previous methods, our approach achieves both more accurate segmentation boundaries and more detailed contextual descriptions that capture object attributes and spatial relationships.

3.2. Data Statistics

Given the limited availability of large-scale 3D scene datasets, it is crucial to leverage multiple existing datasets and apply a unified annotation process to create a comprehensive training corpus. We curate a collection of widely-used 3D indoor scene datasets, including ScanNet [24], ARKitScenes [7], Matterport3D [14], ScanNet++ [99], and Structured3D [107], and apply our proposed pipeline to each. These datasets provide diverse indoor scenes covering both real and synthetic environments, with high-quality RGB-D scans, accurate camera poses, and dense 3D reconstructions, making them ideal for our automatic annotation process.

Through this data pipeline, we create Mosaic3D-5.6M, the largest 3D mask-text paired dataset to date, encompassing over 30K indoor scenes and approximately 1M RGB-D

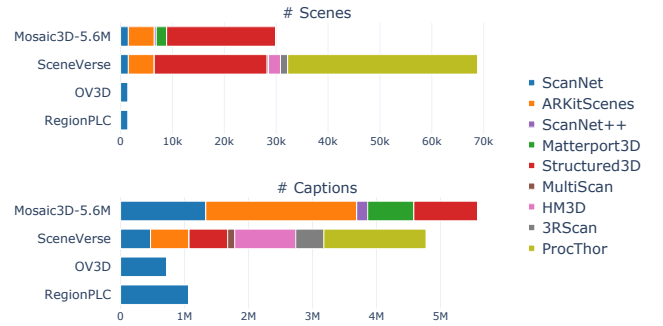


Figure 4. **Statistics of 3D mask-text datasets.** We show the total number of scenes, tokens for generated captions. Our Mosaic3D-5.6M significantly surpasses previous datasets in scale, combining multiple datasets to create the largest 3D mask-text dataset to date.

frames, yielding 5.6M region captions comprising 30M total text tokens. The complete data statistics can be found in Fig. 4. Our dataset offers significant advantages over the existing datasets in terms of:

- **Scale:** We generate over 5.6M mask-text pairs with 30M text tokens across 30K scenes, significantly larger than previous datasets in scene coverage and annotation density.
- **Precision:** Our use of Grounded-SAM [76] and SEEM [110] ensures precise region boundaries, significantly improving over bounding box-based approaches.
- **Richness:** The region-aware VLM generates detailed contextual descriptions that capture both visual attributes and spatial relationships, providing richer semantic information than simple object labels.

4. Mosaic3D Model Training

We train the 3D open-vocabulary segmentation model based on Mosaic3D-5.6M using two-stage training: per-point language alignment (Sec. 4.1), and mask decoder training that predicts instances from these aligned features (Sec. 4.2).

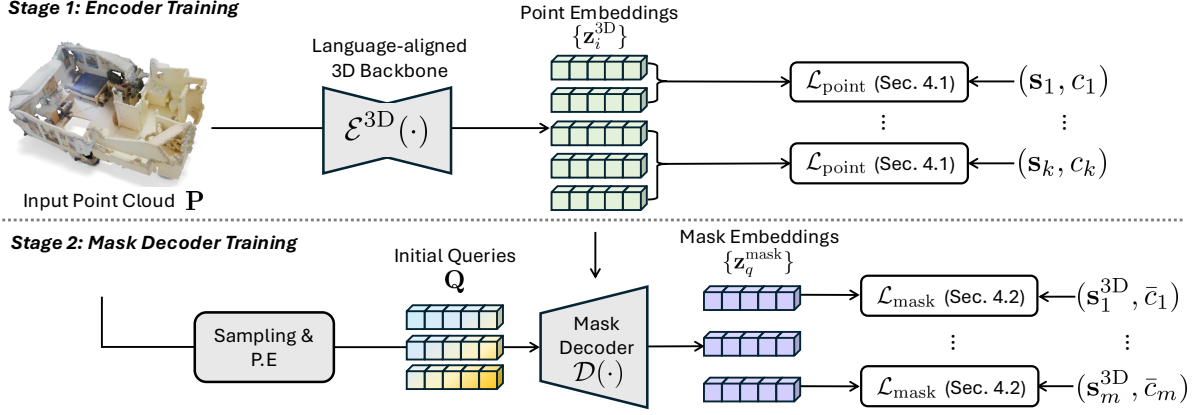


Figure 5. **Mosaic3D model.** Mosaic3D model is a SparseUNet [21] trained with our Mosaic3D-5.6M dataset to extract language-aligned features from 3D point clouds. A mask decoder with positional encodings (P.E) is trained on top to enable instance segmentation.

4.1. Mosaic3D: Language-Aligned 3D Encoder

Architecture. We use U-shaped sparse convnets [21, 33] for our backbone due to their efficiency and scalability. Given a point cloud $\mathbf{P} = \{\mathbf{p}_i\}_{i=1}^N, \mathbf{p}_i \in \mathbb{R}^3$, the network $\mathcal{E}^{3D}(\cdot)$ outputs per-point features $\mathcal{E}^{3D}(\mathbf{P}) = \{\mathbf{z}_i^{3D}\}_{i=1}^N, \mathbf{z}_i^{3D} \in \mathbb{R}^D$.

Training objective. To align the geometric embeddings with language semantics, we employ a contrastive learning framework [27, 98]. Given 3D mask-text pairs $\{(\mathbf{s}_k, c_k)\}_{k=1}^K$, a pre-trained text encoder $\mathcal{E}^{\text{text}}(\cdot)$ computes text embeddings $\mathbf{z}_k^{\text{text}} \in \mathbb{R}^D$ for each caption. The similarity scores between point features and text embeddings are averaged using the region masks to weigh all regions equally. The final training objective is:

$$\mathcal{L}_{\text{point}} = -\frac{1}{K} \sum_{k=1}^K \sum_{i=1}^N (\mathbf{s}_k)_i \log \frac{\exp(\mathbf{z}_i^{3D} \cdot \mathbf{z}_k^{\text{text}} / \tau)}{\sum_{j=1}^K \exp(\mathbf{z}_i^{3D} \cdot \mathbf{z}_j^{\text{text}})} \quad (2)$$

where τ is a learnable logit temperature.

4.2. Mosaic3D with Mask Decoder

On top of our language-aligned backbone, we add a lightweight mask decoder to enable open-vocabulary 3D instance segmentation, avoiding the need for separate instance segmentation networks used in prior work [42, 65, 87, 100].

Architecture. We use Mask3D [82] as our mask decoder, a transformer-based architecture adapted from 2D segmentation [17, 18]. Specifically, our decoder takes non-parametric queries (*i.e.*, positional encodings of points sampled from the input point cloud) and language-aligned point features from our backbone (Sec. 4.1) as input. The decoder outputs mask embeddings aligned with language features, enabling open-vocabulary segmentation of 3D scenes.

Training data. To enable open-vocabulary 3D instance segmentation, we need training data that is not constrained to predefined categories. While prior work [42, 65, 87] used

Algorithm 1 Caption Merging

Require: Our mask-text pairs data $\{(\mathbf{s}_k, c_k)\}_{k=1}^K$, Segment3D [40] masks $\{\mathbf{s}_l^{3D}\}_{l=1}^L$

Ensure: Matched mask-text pairs $\{(\mathbf{s}_m^{3D}, \{c_{j \in \mathcal{M}_m}\})\}_{m=1}^M$

- 1: **for** $k \leftarrow 1$ to K **do**
- 2: $l^* = \arg \max_l \text{IoU}(\mathbf{s}_k, \mathbf{s}_l^{3D})$ ▷ Find match
- 3: **if** \mathcal{M}_{l^*} is not initialized **then**
- 4: $\mathcal{M}_{l^*} \leftarrow \emptyset$ ▷ Initialize empty set
- 5: **end if**
- 6: **if** $\text{IoU}(\mathbf{s}_k, \mathbf{s}_{l^*}^{3D}) > \tau$ **then**
- 7: $\mathcal{M}_{l^*} \leftarrow \mathcal{M}_{l^*} \cup \{k\}$ ▷ Add caption
- 8: **end if**
- 9: **end for**
- 10: **return** $\{(\mathbf{s}_m^{3D}, \{c_{j \in \mathcal{M}_m}\})\}_{m=1}^M$

closed-vocabulary labels, we leverage Segment3D [40]’s class-agnostic masks predicted by SAM [50] and combine them with our multi-view mask-caption data to create a rich open-vocabulary training set. As detailed in Algorithm 1, we merge our mask-caption data $\{(\mathbf{s}_k, c_k)\}_{k=1}^K$ with Segment3D [40] masks $\{\mathbf{s}_l^{3D}\}_{l=1}^L$ based on IoU matching. This yields a set of Segment3D masks $\{(\mathbf{s}_m^{3D}, \{c_{j \in \mathcal{M}_m}\})\}_{m=1}^M$, each associated with multiple captions from our multi-view data. During training, we randomly sample a fixed number of captions for each mask from its associated caption set.

Training objective. Given a point cloud \mathbf{P} and Segment3D masks with associated captions $\{(\mathbf{s}_m^{3D}, \{c_{j \in \mathcal{M}_m}\})\}_{m=1}^M$, we compute Q numbers of mask embeddings $\mathbf{Z}^{\text{mask}} \in \mathbb{R}^{Q \times D}$ and normalized text embeddings $\bar{\mathbf{z}}_m^{\text{text}} \in \mathbb{R}^D$:

$$\mathbf{Z}^{\text{mask}} = \{\mathbf{z}_q^{\text{mask}}\} = \mathcal{D}(\{\mathbf{z}_i^{3D}\}; \mathbf{Q}), \quad \bar{\mathbf{z}}_m^{\text{text}} = \mathcal{E}^{\text{text}}(\bar{c}_m), \quad (3)$$

where $\mathcal{D}(\cdot)$ is our mask decoder that takes point features and sampled queries \mathbf{Q} as input, and \bar{c}_m concatenates all captions associated with mask \mathbf{s}_m^{3D} . Following Segment3D [40], we

first train the mask decoder to predict binary instance masks using three standard losses: objectness prediction loss \mathcal{L}_{obj} , Dice loss $\mathcal{L}_{\text{dice}}$ [62], and binary cross entropy loss \mathcal{L}_{bce} . Then, we use Hungarian matching to find the set of mask predictions that minimizes error given ground-truth masks. The losses are computed as:

$$\mathbf{o} = \text{Linear}(\mathbf{Z}^{\text{mask}}), \quad \mathbf{S} = \sigma(\mathbf{Z}^{\text{mask}} \cdot \mathbf{Z}^{3\text{DT}}), \quad (4)$$

where $\mathbf{o} \in \mathbb{R}^{Q \times 2}$ and $\mathbf{S} \in \mathbb{R}^{Q \times N}$ are objectness scores and predicted binary masks. To enable open-vocabulary segmentation, we introduce a mask caption loss \mathcal{L}_{cap} that explicitly aligns mask embeddings with caption embeddings:

$$\mathcal{L}_{\text{cap}} = -\frac{1}{M} \sum_{m=1}^M \log \frac{\exp(\mathbf{z}_m^{\text{mask}} \cdot \bar{\mathbf{z}}_k^{\text{text}} / \tau)}{\sum_{j=1}^M \exp(\mathbf{z}_m^{\text{mask}} \cdot \bar{\mathbf{z}}_j^{\text{text}})} \quad (5)$$

The total loss is $\mathcal{L}_{\text{mask}} = \lambda_{\text{obj}} \mathcal{L}_{\text{obj}} + \lambda_{\text{dice}} \mathcal{L}_{\text{dice}} + \lambda_{\text{bce}} \mathcal{L}_{\text{bce}} + \lambda_{\text{cap}} \mathcal{L}_{\text{cap}}$, where in practice we set $\lambda_{\text{obj}} = 2$, $\lambda_{\text{dice}} = 5$, $\lambda_{\text{bce}} = 2$, and $\lambda_{\text{cap}} = 1$. With this loss, our language-aligned mask decoder enables direct open-vocabulary 3D segmentation, avoiding the expensive multi-view CLIP inference required by prior methods [42, 65, 87].

5. Experiments

In this section, we investigate how dataset size impacts model performance (Sec. 5.2). Next, we benchmark Mosaic3D against existing methods for open-vocabulary 3D scene segmentation (Sec. 5.3). Finally, we analyze our system through attention visualization, zero-shot experiments, and ablation studies on the Mosaic3D-5.6M data engine (Sec. 5.4).

5.1. Setup

Implementation details. We adopt Sparse ConvNets [21, 33] as our 3D encoder, leveraging their efficiency in processing sparse 3D data. Our baseline architecture uses SparseUNet34C [21] with 43.7M trainable parameters. For text encoder, we employ Recap-CLIP [55], which is pre-trained on longer re-captioned datasets, enabling better processing of the long captions in our dataset. For training, we use SGD optimization [9] with an initial learning rate of 0.05 and a weight decay of 1×10^{-4} , coupled with the OneCycleLR scheduler [84], with batch size 4. To enhance multi-data joint training, we adopt recent technique of Point Prompt Training (PPT) [95]. All models are trained for 128 epochs on eight A100 GPUs. For instance segmentation, we fine-tune the pre-trained Mosaic3D model with an additional mask decoder on Mosaic3D-5.6M with caption merging (Alg. 1). Please refer to the appendix for more details.

Evaluation metrics. We evaluate performance using mean Intersection over Union (mIoU) and mean Accuracy (mAcc), which are standard metrics for open-vocabulary 3D semantic segmentation. Following prior work [27, 48, 98], we report f-mIoU and f-mAcc metrics that exclude background classes.

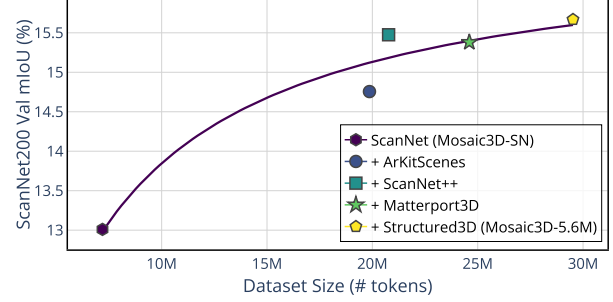


Figure 6. **Model performance scales with training data.** We observe consistent improvements in open-vocabulary semantic segmentation on ScanNet200 [78] as we increase the amount of training data. This shows the value of our large-scale data generation pipeline in improving open-vocabulary 3D scene understanding.

5.2. Impact of Dataset Size

To understand how the size of the training data affects model performance, we conduct experiments with varying amounts of training data. Specifically, we gradually increase the training data by adding one dataset at a time in the following order: ScanNet [24], ARKitScenes [7], ScanNet++ [99], Matterport3D [14], and Structured3D [107]. For these experiments, we fix the model architecture to SparseUNet34C [21]. All other hyperparameters remain fixed across the experiments. As shown in Fig. 6, increasing the size of the dataset generally improves the accuracy of open-vocabulary semantic segmentation on the ScanNet200 benchmark [78]. The most significant performance gains are observed when incorporating ARKitScenes and ScanNet++, which we attribute to their high-quality, dense RGB-D frames captured from real 3D environments. From here on, we refer to our Mosaic3D model as the model jointly trained on all datasets.

5.3. Benchmark Results

Open-vocabulary 3D semantic segmentation. We evaluate on ScanNet20 validation set, ScanNet200 validation set, Matterport3D test set, and ScanNet++ validation set, following prior work [27, 48, 68, 98]. These datasets contain 20, 200, 160, and 100 semantic classes respectively, providing diverse benchmarks for open-vocabulary 3D semantic segmentation. Using only ScanNet training data, Mosaic3D outperforms prior work in terms of f-mIoU (%) on all benchmarks: surpassing OV3D [48] by 1.0p on ScanNet20 and RegionPLC [98] by 4.9p, 2.4p, and 3.8p on ScanNet++, Matterport3D, and ScanNet200 respectively. Training on our full dataset Mosaic3D-5.6M further improves f-mIoU (%) across all benchmarks, achieving 68.1 on ScanNet20, 18.0 on ScanNet++, 13.1 on Matterport3D, and 15.7 on ScanNet200. Notably, our approach achieves 7.1p higher f-mIoU than SceneVerse [44] despite using fewer scenes, highlighting the importance of caption quantity per scene.

Open-vocabulary 3D instance segmentation. As shown

Method	Source Datasets	ScanNet20 (20)		ScanNet++ (100)		Matterport3D (160)		ScanNet200 (200)	
		f-mIoU	f-mAcc	f-mIoU	f-mAcc	f-mIoU	f-mAcc	f-mIoU	f-mAcc
OpenScene-3D [†] [68]	ScanNet [24]	57.5	72.4	8.8	14.7	5.7	10.7	6.4	12.2
PLA [27]	ScanNet [24]	19.1	41.5	-	-	-	-	1.8	3.1
RegionPLC [98]	ScanNet [24]	59.6	77.5	-	-	-	-	9.1	17.3
RegionPLC ^o [98]	ScanNet [24]	55.6	76.3	11.3	20.1	6.2	13.3	9.2	16.4
OV3D [48]	ScanNet [24]	64.0	76.3	-	-	-	-	8.7	-
Mosaic3D	ScanNet [24]	65.0	82.5	16.2	27.1	8.6	17.8	13.0	24.5
RegionPLC [98] + SceneVerse [44]	MS [61] + 3RS [92] + SN [24] + AR [7] + HM3D [72] + S3D [107] + PT [25]	61.0	79.7	-	-	-	-	-	-
Mosaic3D	SN [24] + AR [7] + SN2 [99] + M [14] + S3D [107]	68.1	84.4	18.0	29.0	13.1	27.7	15.7	28.3

Table 1. **Annotation-free 3D semantic segmentation on ScanNet [24, 78], Matterport3D [14], and ScanNet++ [99].** We report f-mIoU and f-mAcc excluding background classes (wall, floor, ceiling), following [27, 44, 68, 98]. [†] denotes official checkpoints and ^o denotes our reproductions. The numbers in parentheses indicate the total number of classes in each dataset. Dataset abbreviations SN, AR, SN2, M, S3D, MS, 3RS, HM3D, and PT denote ScanNet [24], ARKitScenes [7], ScanNet++ [99], Matterport3D [14], Structured3D [107], MultiScan [61], 3RScan [92], Habitat-Matterport 3D [72], and ProcTHOR [25], respectively.

	Method	Inputs	3D Region Proposal Network	mAP	mAP ₅₀	mAP ₂₅	mAP _{head}	mAP _{com.}	mAP _{tail}	Latency
(a)	Open3DIS [65]	3D + 2D	Superpoints [29] + ISBNet [64] + Grounded-SAM [76]	23.7	29.4	32.8	27.8	21.2	21.8	33.5
	SAI3D [100]	3D + 2D	Superpoints [29] + SAM [50]	12.7	18.8	24.1	12.1	10.4	16.2	75.2
(b)	OpenScene-2D [68]	3D + 2D	Mask3D [82]	11.7	15.2	17.8	13.4	11.6	9.9	-
	OpenScene-2D/3D [68]	3D + 2D	Mask3D [82]	5.3	6.7	8.1	11.0	3.2	1.1	-
	OpenMask3D [87]	3D + 2D	Mask3D [82]	15.4	19.9	23.1	17.1	14.1	14.9	47.3
(c)	OpenScene-3D [68]	3D	Mask3D [82]	4.8	6.2	7.2	10.6	2.6	0.7	1.1
	RegionPLC [98]	3D	Mask3D [82]	6.3	8.6	9.7	15.6	1.0	1.7	1.0
	OpenIns3D [42]	3D	Mask3D [82]	8.8	10.3	14.4	16.0	6.5	4.2	285.2
	OpenIns3D [†] [42]	3D	Mask3D [82]	3.3	5.0	5.6	7.0	1.4	1.2	50.0
	Mosaic3D	3D	Mask3D [82]	11.8	16.0	17.8	21.8	7.2	5.4	1.0
(d)	OpenScene-3D [68]	3D	Segment3D [40]	0.6	1.0	1.6	1.4	0.4	0.0	2.0
	RegionPLC [98]	3D	Segment3D [40]	1.5	2.1	2.6	2.3	0.2	1.9	1.9
	OpenIns3D [†] [42]	3D	Segment3D [40]	1.7	2.7	3.7	3.2	0.8	1.0	64.8
	Mosaic3D	3D	Segment3D [40]	2.7	4.2	5.7	3.8	2.0	2.4	1.9
	Mosaic3D w/ Decoder	3D	X	3.9	7.0	12.3	6.6	2.1	2.8	1.2

Table 2. **Annotation-free 3D instance segmentation on ScanNet200 [78].** For a fair comparison, we categorize methods by input types and region proposal network: (a) Methods using both 3D point cloud and 2D RGB-D images, with 3D+2D region proposals and 2D CLIP inference. (b) Methods using both 3D+2D inputs, with region proposals from Mask3D [82] (closed-vocab) and 2D CLIP inference. (c) Methods using only 3D input with Mask3D [82]. (d) Methods using only 3D input with open-vocabulary 3D region proposals. [†] denotes results without test-time voting, following the official implementation. Latency reports runtime (seconds) per scene on ScanNet validation.

in Table 2, methods using both 2D and 3D inputs achieve strong results by directly applying CLIP models, but are impractical due to high latency (33-285 sec per scene) from processing multiple view images. For fair comparison, we evaluate our Mosaic3D trained only on ScanNet against prior methods [42, 65, 68, 87, 98, 100] that also train and evaluate on ScanNet. With Mask3D [82] as a closed-vocabulary region proposal network, Mosaic3D outperforms the previous best method OpenIns3D [42] by 3.0p mAP. When using truly open-vocabulary Segment3D [40] proposals, Mosaic3D maintains strong performance at 2.7 mAP despite the more challenging setting. Finally, our lightweight mask decoder trained with Mosaic3D-5.6M with caption merging (Alg. 1) achieves 3.9 mAP while being the first single-stage open-vocabulary 3D instance segmentation model that does not require ground truth labels.

5.4. Analysis

Data engine components. Finally, we conduct an ablation study on different component combinations of Mosaic3D data engine to measure the contribution of each component. To understand the impact of different components in our data generation pipeline, we conduct ablation experiments by systematically varying key components while keeping the model architecture (SparseUNet16 [98]) and source dataset (ScanNet only) fixed. As shown in Table 3, we evaluate the following configurations:

- **Mask Generation:** We compare our Grounded-SAM [76] + SEEM [110] approach against using only Grounded-SAM [76] or SEEM [110]. Results show that combining both methods leads to better region proposals.
- **Caption Generation:** We compare LLaVA [58] for image-

Segmentation	Captioning	# frames (K)	ScanNet20 [24]				ScanNet200 [78]			
			mIoU	mAcc	f-mIoU	f-mAcc	mIoU	mAcc	f-mIoU	f-mAcc
Detic [108]	Kosmos-2 [69]	125	32.7	64.1	52.3	73.2	6.2	14.1	7.4	14.2
LLaVA-1.5 [57] + SEEM [110]	LLaVA-1.5 [57]	25	30.1	61.9	45.9	68.1	4.6	13.0	5.7	13.0
RAM++ [41] + SEEM [110]	LLaVA-1.5 [57]	25	41.3	67.1	57.0	74.6	6.8	13.2	7.4	13.2
RAM++ [41] + Grounded-SAM [50, 76]	Ferret [101]	25	41.9	71.1	59.6	79.2	8.2	17.8	9.0	17.8
RAM++ [41] + Grounded-SAM [50, 76]	Osprey [103]	25	46.2	72.0	63.7	80.7	8.4	18.2	9.2	18.2
RAM++ [41] + Grounded-SAM2 [75, 76]	Osprey [103]	25	45.1	71.3	62.3	79.7	9.5	20.0	10.6	20.3
RAM++ [41] + Grounded-SAM2 [75, 76]	Osprey [103]	125	46.1	73.0	65.0	81.6	10.2	21.2	11.5	21.3
RAM++ [41] + Grounded-SAM2 [75, 76] & SEEM [110]	Osprey [103]	125	50.0	73.7	65.2	82.0	10.5	20.2	11.0	20.1

Table 3. **Data pipeline comparison.** We evaluate data generation pipelines for annotation-free 3D semantic segmentation on ScanNet20 [24] and ScanNet200 [78]. All experiments use RegionPLC’s [98] architecture and training objective.

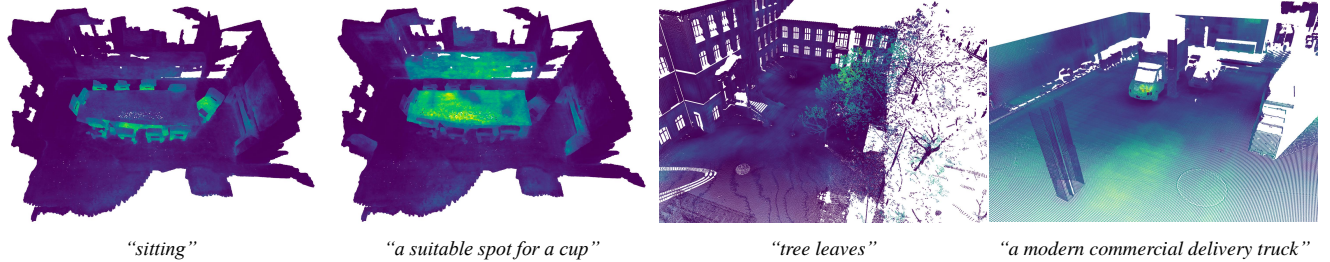


Figure 7. **Attention visualization of Mosaic3D as a 3D foundational model.** From left to right, the first two examples show results on ScanNet [24], while the next two examples show results on ETH3D [80]. More examples are provided in the supplementary material.

level captioning against Ferret [101] and Osprey [103] for region-level captioning. Region-level approaches perform better by providing detailed per-region descriptions, with Osprey achieving the best results.

Our final pipeline combines Grounded-SAM2 [75, 76] with SEEM [110] for mask generation and Osprey [103] for captioning, as this configuration yields optimal performance.

Attention visualization. In Fig. 7, we visualize the similarity between dense point features obtained from Mosaic3D and free-form text queries. As shown in the figure, despite being trained only on indoor scenes, Mosaic3D effectively localizes semantic regions described by text queries across both indoor [24] and outdoor [80] datasets.

Zero-shot 3D semantic segmentation. While annotation-free methods [48, 98] do not utilize GT annotations, their generated captions often contain class names from the evaluation set (e.g., "chair"), making them not truly "zero-shot." To address this, we conduct a more rigorous zero-shot analysis by anonymizing all class names in the training captions, replacing them with general terms like "object." To ensure fair comparison, we kept all experimental settings (e.g., model architecture, CLIP model, loss function) identical across methods, varying only the training data. As shown in Table 4, all models experience performance drops when trained on anonymized data, but the model trained on Mosaic3D-5.6M maintains the strongest performance (10.5 f-mIoU), outperforming both annotation-free methods and approaches that use ground truth annotations like LEO [39].

Dataset	f-mIoU		Δ
	w/o Anon.	w/ Anon.	
RegionPLC [98]	8.5	3.8	↓ 4.7
OV3D ^b [48]	9.2	4.3	↓ 4.9
Mosaic3D-SN ¹	13.0	8.7	↓ 4.3
LEO [39]	14.8	2.9	↓ 11.9
SceneVerse [44]	13.6	4.7	↓ 8.9
EmbodiedScan [94]	6.7	0.0	↓ 6.7
MMScan [60]	11.7	8.5	↓ 3.2
Mosaic3D-5.6M	15.7	10.5	↓ 5.2

Table 4. **Zero-shot semantic segmentation on ScanNet200 [78].** "Anon." refers to class name anonymization, and ^b indicates our re-implementation of OV3D as the original data is not available.

6. Conclusion

In this work, we introduced a comprehensive approach for open-vocabulary 3D scene understanding that addresses fundamental data and modeling challenges in the field. Our key contribution is a novel dataset generation pipeline that leverages state-of-the-art 2D visual foundation models to create high-quality 3D mask-text pairs, enabling the creation of Mosaic3D-5.6M, the largest open-vocabulary 3D scene dataset to date with 5.6M captions. Building on this data, we developed a model that combines Mosaic3D, a language-aligned 3D encoder, with a lightweight mask decoder, achieving state-of-the-art results on open-vocabulary 3D segmentation tasks. Our ablation studies demonstrate the importance of dataset scale and annotation quality for open-vocabulary 3D understanding, providing a foundation for leveraging 2D vision models in 3D scene understanding.

¹A subset of Mosaic3D-5.6M using only ScanNet as source dataset

Acknowledgement. This work was partly supported by the Institute of Information & Communications Technology Planning & Evaluation (IITP) grants (RS-2021-II212068: AI Innovation Hub, RS-2024-00457882: National AI Research Lab Project) funded by the Korea government (MSIT).

References

- [1] Vit-gpt2 image captioning. <https://huggingface.co/nlpconnect/vit-gpt2-image-captioning>, 2022. 2, 3
- [2] Josh Achiam, Steven Adler, Sandhini Agarwal, Lama Ahmad, Ilge Akkaya, Florencia Leoni Aleman, Diogo Almeida, Janko Altschmidt, Sam Altman, Shyamal Anadkat, et al. Gpt-4 technical report. *arXiv preprint arXiv:2303.08774*, 2023. 2
- [3] Panos Achlioptas, Ahmed Abdelreheem, Fei Xia, Mohamed Elhoseiny, and Leonidas J. Guibas. ReferIt3D: Neural listeners for fine-grained 3d object identification in real-world scenes. In *16th European Conference on Computer Vision (ECCV)*, 2020. 2
- [4] Daichi Azuma, Taiki Miyanishi, Shuhei Kurita, and Motoaki Kawanabe. Scanqa: 3d question answering for spatial scene understanding. In *proceedings of the IEEE/CVF conference on computer vision and pattern recognition*, pages 19129–19139, 2022. 2
- [5] Jinze Bai, Shuai Bai, Yunfei Chu, Zeyu Cui, Kai Dang, Xiaodong Deng, Yang Fan, Wenbin Ge, Yu Han, Fei Huang, et al. Qwen technical report. *arXiv preprint arXiv:2309.16609*, 2023. 2
- [6] Jinze Bai, Shuai Bai, Shusheng Yang, Shijie Wang, Sinan Tan, Peng Wang, Junyang Lin, Chang Zhou, and Jingren Zhou. Qwen-vl: A versatile vision-language model for understanding, localization, text reading, and beyond. *arXiv preprint arXiv:2308.12966*, 2023. 2
- [7] Gilad Baruch, Zhuoyuan Chen, Afshin Dehghan, Yuri Feigin, Peter Fu, Thomas Gebauer, Daniel Kurz, Tal Dimry, Brandon Joffe, Arik Schwartz, et al. Arkitscenes: A diverse real-world dataset for 3d indoor scene understanding using mobile rgb-d data. In *Thirty-fifth Conference on Neural Information Processing Systems Datasets and Benchmarks Track (Round 1)*, 2021. 1, 2, 4, 6, 7, 5
- [8] Zalan Borsos, Raphaël Marinier, Damien Vincent, Eugene Kharitonov, Olivier Pietquin, Matt Sharifi, Dominik Roblek, Olivier Teboul, David Grangier, Marco Tagliasacchi, et al. Audioldm: A language modeling approach to audio generation. *IEEE/ACM Transactions on Audio, Speech, and Language Processing*, 31:2523–2533, 2023. 2
- [9] Léon Bottou. Large-scale machine learning with stochastic gradient descent. In *Proceedings of COMPSTAT'2010: 19th International Conference on Computational StatisticsParis France, August 22-27, 2010 Keynote, Invited and Contributed Papers*, pages 177–186. Springer, 2010. 6
- [10] Tom B Brown. Language models are few-shot learners. *arXiv preprint arXiv:2005.14165*, 2020. 2
- [11] Minwoo Byeon, Beomhee Park, Haecheon Kim, Sungjun Lee, Woonhyuk Baek, and Saehoon Kim. Coyo-700m: Image-text pair dataset. <https://github.com/kakaobrain/coyo-dataset>, 2022. 1
- [12] Nicolas Carion, Francisco Massa, Gabriel Synnaeve, Nicolas Usunier, Alexander Kirillov, and Sergey Zagoruyko. End-to-end object detection with transformers. In *European conference on computer vision*, pages 213–229. Springer, 2020. 2
- [13] Mathilde Caron, Hugo Touvron, Ishan Misra, Hervé Jégou, Julien Mairal, Piotr Bojanowski, and Armand Joulin. Emerging properties in self-supervised vision transformers. In *Proceedings of the IEEE/CVF international conference on computer vision*, pages 9650–9660, 2021. 2
- [14] Angel Chang, Angela Dai, Thomas Funkhouser, Maciej Halber, Matthias Nießner, Manolis Savva, Shuran Song, Andy Zeng, and Yinda Zhang. Matterport3d: Learning from rgb-d data in indoor environments. In *2017 International Conference on 3D Vision (3DV)*, pages 667–676. IEEE Computer Society, 2017. 1, 2, 4, 6, 7, 5
- [15] Dave Zhenyu Chen, Angel X Chang, and Matthias Nießner. Scanrefer: 3d object localization in rgb-d scans using natural language. In *European conference on computer vision*, pages 202–221. Springer, 2020. 2, 4, 5
- [16] Xi Chen, Xiao Wang, Soravit Changpinyo, AJ Piergiovanni, Piotr Padlewski, Daniel Salz, Sebastian Goodman, Adam Grycner, Basil Mustafa, Lucas Beyer, et al. Pali: A jointly-scaled multilingual language-image model. In *The Eleventh International Conference on Learning Representations*, 2022. 1
- [17] Bowen Cheng, Alexander G Schwing, and Alexander Kirillov. Per-pixel classification is not all you need for semantic segmentation. In *35th Conference on Neural Information Processing Systems, NeurIPS 2021*, pages 17864–17875. Neural information processing systems foundation, 2021. 2, 5
- [18] Bowen Cheng, Ishan Misra, Alexander G Schwing, Alexander Kirillov, and Rohit Girdhar. Masked-attention mask transformer for universal image segmentation. In *Proceedings of the IEEE/CVF conference on computer vision and pattern recognition*, pages 1290–1299, 2022. 2, 5
- [19] Wei-Lin Chiang, Zhuohan Li, Zi Lin, Ying Sheng, Zhanghao Wu, Hao Zhang, Lianmin Zheng, Siyuan Zhuang, Yonghao Zhuang, Joseph E. Gonzalez, Ion Stoica, and Eric P. Xing. Vicuna: An open-source chatbot impressing gpt-4 with 90%* chatgpt quality, 2023. 2
- [20] Seokju Cho, Heeseong Shin, Sunghwan Hong, Anurag Arnab, Paul Hongsuck Seo, and Seungryong Kim. Catseg: Cost aggregation for open-vocabulary semantic segmentation. In *Proceedings of the IEEE/CVF Conference on Computer Vision and Pattern Recognition*, pages 4113–4123, 2024. 2
- [21] Christopher Choy, JunYoung Gwak, and Silvio Savarese. 4d spatio-temporal convnets: Minkowski convolutional neural networks. In *Proceedings of the IEEE Conference on Computer Vision and Pattern Recognition*, pages 3075–3084, 2019. 5, 6, 3
- [22] Hyung Won Chung, Le Hou, Shayne Longpre, Barret Zoph, Yi Tay, William Fedus, Yunxuan Li, Xuezhi Wang, Mostafa

- Dehghani, Siddhartha Brahma, et al. Scaling instruction-finetuned language models. *Journal of Machine Learning Research*, 25(70):1–53, 2024. 2
- [23] Pointcept Contributors. Pointcept: A codebase for point cloud perception research. <https://github.com/Pointcept/Pointcept>, 2023. 2
- [24] Angela Dai, Angel X Chang, Manolis Savva, Maciej Halber, Thomas Funkhouser, and Matthias Nießner. Scannet: Richly-annotated 3d reconstructions of indoor scenes. In *Proceedings of the IEEE conference on computer vision and pattern recognition*, pages 5828–5839, 2017. 1, 2, 4, 6, 7, 8, 3, 5
- [25] Matt Deitke, Eli VanderBilt, Alvaro Herrasti, Luca Weihs, Kiana Ehsani, Jordi Salvador, Winson Han, Eric Kolve, Aniruddha Kembhavi, and Roozbeh Mottaghi. Proctor: Large-scale embodied ai using procedural generation. *Advances in Neural Information Processing Systems*, 35:5982–5994, 2022. 7
- [26] Soham Deshmukh, Benjamin Elizalde, Rita Singh, and Huaming Wang. Pengi: An audio language model for audio tasks. *Advances in Neural Information Processing Systems*, 36:18090–18108, 2023. 2
- [27] Runyu Ding, Jihan Yang, Chuhui Xue, Wenqing Zhang, Song Bai, and Xiaojuan Qi. Pla: Language-driven open-vocabulary 3d scene understanding. In *Proceedings of the IEEE/CVF Conference on Computer Vision and Pattern Recognition*, 2023. 2, 3, 5, 6, 7
- [28] Abhimanyu Dubey, Abhinav Jauhri, Abhinav Pandey, Abhishek Kadian, Ahmad Al-Dahle, Aiesha Letman, Akhil Mathur, Alan Schelten, Amy Yang, Angela Fan, et al. The llama 3 herd of models. *arXiv preprint arXiv:2407.21783*, 2024. 2
- [29] Pedro F Felzenszwalb and Daniel P Huttenlocher. Efficient graph-based image segmentation. *International journal of computer vision*, 59:167–181, 2004. 7
- [30] Samir Yitzhak Gadre, Gabriel Ilharco, Alex Fang, Jonathan Hayase, Georgios Smyrnis, Thao Nguyen, Ryan Marten, Mitchell Wortsman, Dhruva Ghosh, Jieyu Zhang, et al. Datcomp: In search of the next generation of multimodal datasets. *Advances in Neural Information Processing Systems*, 36, 2024. 1
- [31] Golnaz Ghiasi, Xiuye Gu, Yin Cui, and Tsung-Yi Lin. Scaling open-vocabulary image segmentation with image-level labels. In *European Conference on Computer Vision*, pages 540–557. Springer, 2022. 1, 2
- [32] Rohit Girdhar, Alaaeldin El-Nouby, Zhuang Liu, Mannat Singh, Kalyan Vasudev Alwala, Armand Joulin, and Ishan Misra. Imagebind one embedding space to bind them all. In *IEEE/CVF Conference on Computer Vision and Pattern Recognition, CVPR 2023, Vancouver, BC, Canada, June 17-24, 2023*, pages 15180–15190. IEEE, 2023. 2
- [33] Benjamin Graham, Martin Engelcke, and Laurens Van Der Maaten. 3d semantic segmentation with submanifold sparse convolutional networks. In *Proceedings of the IEEE conference on computer vision and pattern recognition*, pages 9224–9232, 2018. 5, 6
- [34] Xiuye Gu, Tsung-Yi Lin, Weicheng Kuo, and Yin Cui. Open-vocabulary object detection via vision and language knowledge distillation. In *International Conference on Learning Representations*, 2021. 1
- [35] Qiushan Guo, Shalini De Mello, Hongxu Yin, Wonmin Byeon, Ka Chun Cheung, Yizhou Yu, Ping Luo, and Sifei Liu. Regionpt: Towards region understanding vision language model. *arXiv preprint arXiv:2403.02330*, 2024. 2
- [36] Kaiming He, Xiangyu Zhang, Shaoqing Ren, and Jian Sun. Deep residual learning for image recognition. In *Proceedings of the IEEE conference on computer vision and pattern recognition*, pages 770–778, 2016. 3
- [37] Jonathan Ho, Ajay Jain, and Pieter Abbeel. Denoising diffusion probabilistic models. *Advances in neural information processing systems*, 33:6840–6851, 2020. 2
- [38] Xiaowei Hu, Zhe Gan, Jianfeng Wang, Zhengyuan Yang, Zicheng Liu, Yumao Lu, and Lijuan Wang. Scaling up vision-language pre-training for image captioning. In *Proceedings of the IEEE/CVF conference on computer vision and pattern recognition*, pages 17980–17989, 2022. 1
- [39] Jiangyong Huang, Silong Yong, Xiaojian Ma, Xiongkun Linghu, Puhao Li, Yan Wang, Qing Li, Song-Chun Zhu, Baoxiong Jia, and Siyuan Huang. An Embodied Generalist Agent in 3D World, 2023. 8
- [40] Rui Huang, Songyou Peng, Ayca Takmaz, Federico Tombari, Marc Pollefeys, Shiji Song, Gao Huang, and Francis Engelmann. Segment3d: Learning fine-grained class-agnostic 3d segmentation without manual labels. In *European Conference on Computer Vision*, 2024. 2, 5, 7
- [41] Xinyu Huang, Yi-Jie Huang, Youcai Zhang, Weiwei Tian, Rui Feng, Yuejie Zhang, Yanchun Xie, Yaqian Li, and Lei Zhang. Open-set image tagging with multi-grained text supervision. *arXiv e-prints*, pages arXiv–2310, 2023. 2, 3, 8, 4
- [42] Zhening Huang, Xiaoyang Wu, Xi Chen, Hengshuang Zhao, Lei Zhu, and Joan Lasenby. Openins3d: Snap and lookup for 3d open-vocabulary instance segmentation. In *European Conference on Computer Vision*, 2024. 2, 5, 6, 7
- [43] Jitesh Jain, Jiachen Li, Mang Tik Chiu, Ali Hassani, Nikita Orlov, and Humphrey Shi. Oneformer: One transformer to rule universal image segmentation. In *Proceedings of the IEEE/CVF Conference on Computer Vision and Pattern Recognition*, pages 2989–2998, 2023. 2
- [44] Baoxiong Jia, Yixin Chen, Huangyue Yu, Yan Wang, Xuesong Niu, Tengyu Liu, Qing Li, and Siyuan Huang. SceneVerse: Scaling 3D Vision-Language Learning for Grounded Scene Understanding, 2024. 2, 6, 7, 8
- [45] Chao Jia, Yinfei Yang, Ye Xia, Yi-Ting Chen, Zarana Parekh, Hieu Pham, Quoc Le, Yun-Hsuan Sung, Zhen Li, and Tom Duerig. Scaling up visual and vision-language representation learning with noisy text supervision. In *International conference on machine learning*, pages 4904–4916. PMLR, 2021. 2
- [46] Albert Q Jiang, Alexandre Sablayrolles, Arthur Mensch, Chris Bamford, Devendra Singh Chaplot, Diego de las Casas, Florian Bressand, Gianna Lengyel, Guillaume Lample, Lucile Saulnier, et al. Mistral 7b. *arXiv preprint arXiv:2310.06825*, 2023. 2

- [47] Albert Q Jiang, Alexandre Sablayrolles, Antoine Roux, Arthur Mensch, Blanche Savary, Chris Bamford, Devendra Singh Chaplot, Diego de las Casas, Emma Bou Hanna, Florian Bressand, et al. Mixtral of experts. *arXiv preprint arXiv:2401.04088*, 2024. 2
- [48] Li Jiang, Shaoshuai Shi, and Bernt Schiele. Open-vocabulary 3d semantic segmentation with foundation models. In *Proceedings of the IEEE/CVF Conference on Computer Vision and Pattern Recognition*, pages 21284–21294, 2024. 2, 3, 6, 7, 8, 1, 4
- [49] Dahyun Kang and Minsu Cho. In defense of lazy visual grounding for open-vocabulary semantic segmentation. In *European Conference on Computer Vision*, 2024. 2
- [50] Alexander Kirillov, Eric Mintun, Nikhila Ravi, Hanzi Mao, Chloe Rolland, Laura Gustafson, Tete Xiao, Spencer Whitehead, Alexander C Berg, Wan-Yen Lo, et al. Segment anything. In *Proceedings of the IEEE/CVF International Conference on Computer Vision*, pages 4015–4026, 2023. 2, 3, 4, 5, 7, 8
- [51] Boyi Li, Kilian Q Weinberger, Serge Belongie, Vladlen Koltun, and Rene Ranftl. Language-driven semantic segmentation. In *International Conference on Learning Representations*, 2022. 1, 2
- [52] Feng Li, Hao Zhang, Peize Sun, Xueyan Zou, Shilong Liu, Jianwei Yang, Chunyuan Li, Lei Zhang, and Jianfeng Gao. Semantic-sam: Segment and recognize anything at any granularity. In *European Conference on Computer Vision*, 2024. 2
- [53] Junnan Li, Dongxu Li, Caiming Xiong, and Steven C. H. Hoi. BLIP: bootstrapping language-image pre-training for unified vision-language understanding and generation. In *International Conference on Machine Learning, ICML 2022, 17-23 July 2022, Baltimore, Maryland, USA*, pages 12888–12900. PMLR, 2022. 1
- [54] Junnan Li, Dongxu Li, Silvio Savarese, and Steven C. H. Hoi. BLIP-2: bootstrapping language-image pre-training with frozen image encoders and large language models. In *International Conference on Machine Learning, ICML 2023, 23-29 July 2023, Honolulu, Hawaii, USA*, pages 19730–19742. PMLR, 2023.
- [55] Xianhang Li, Haoqin Tu, Mude Hui, Zeyu Wang, Bingchen Zhao, Junfei Xiao, Sucheng Ren, Jieru Mei, Qing Liu, Huangjie Zheng, et al. What if we recaption billions of web images with llama-3? *arXiv preprint arXiv:2406.08478*, 2024. 6, 4
- [56] Feng Liang, Bichen Wu, Xiaoliang Dai, Kunpeng Li, Yinan Zhao, Hang Zhang, Peizhao Zhang, Peter Vajda, and Diana Marculescu. Open-vocabulary semantic segmentation with mask-adapted clip. In *Proceedings of the IEEE/CVF Conference on Computer Vision and Pattern Recognition*, pages 7061–7070, 2023. 1
- [57] Haotian Liu, Chunyuan Li, Yuheng Li, and Yong Jae Lee. Improved baselines with visual instruction tuning. In *Proceedings of the IEEE/CVF Conference on Computer Vision and Pattern Recognition*, pages 26296–26306, 2024. 8, 2
- [58] Haotian Liu, Chunyuan Li, Qingyang Wu, and Yong Jae Lee. Visual instruction tuning. In *Advances in neural information processing systems*, 2024. 2, 3, 7
- [59] Shilong Liu, Zhaoyang Zeng, Tianhe Ren, Feng Li, Hao Zhang, Jie Yang, Qing Jiang, Chunyuan Li, Jianwei Yang, Hang Su, et al. Grounding dino: Marrying dino with grounded pre-training for open-set object detection. *arXiv preprint arXiv:2303.05499*, 2023. 2, 3
- [60] Ruiyuan Lyu, Jingli Lin, Tai Wang, Xiaohan Mao, Yilun Chen, Runsen Xu, Haifeng Huang, Chenming Zhu, Dahua Lin, and Jiangmiao Pang. Mmscan: A multi-modal 3d scene dataset with hierarchical grounded language annotations. *Advances in Neural Information Processing Systems*, 37: 50898–50924, 2024. 2, 8
- [61] Yongsun Mao, Yiming Zhang, Hanxiao Jiang, Angel Chang, and Manolis Savva. Multiscan: Scalable rgbd scanning for 3d environments with articulated objects. *Advances in neural information processing systems*, 35:9058–9071, 2022. 7
- [62] Fausto Milletari, Nassir Navab, and Seyed-Ahmad Ahmadi. V-net: Fully convolutional neural networks for volumetric medical image segmentation. In *2016 fourth international conference on 3D vision (3DV)*, pages 565–571. Ieee, 2016. 6
- [63] Muhammad Ferjad Naeem, Yongqin Xian, Xiaohua Zhai, Lukas Hoyer, Luc Van Gool, and Federico Tomba. Silc: Improving vision language pretraining with self-distillation. In *European Conference on Computer Vision*, 2024. 2
- [64] Tuan Duc Ngo, Binh-Son Hua, and Khoi Nguyen. Isbnet: a 3d point cloud instance segmentation network with instance-aware sampling and box-aware dynamic convolution. In *Proceedings of the IEEE/CVF Conference on Computer Vision and Pattern Recognition*, pages 13550–13559, 2023. 7
- [65] Phuc Nguyen, Tuan Duc Ngo, Evangelos Kalogerakis, Chuang Gan, Anh Tran, Cuong Pham, and Khoi Nguyen. Open3dis: Open-vocabulary 3d instance segmentation with 2d mask guidance. In *Proceedings of the IEEE/CVF Conference on Computer Vision and Pattern Recognition*, pages 4018–4028, 2024. 2, 5, 6, 7
- [66] Alexander Quinn Nichol and Prafulla Dhariwal. Improved denoising diffusion probabilistic models. In *International conference on machine learning*, pages 8162–8171. PMLR, 2021. 2
- [67] Maxime Oquab, Timothée Darcet, Théo Moutakanni, Huy V. Vo, Marc Szafraniec, Vasil Khalidov, Pierre Fernandez, Daniel HAZIZA, Francisco Massa, Alaaeldin El-Nouby, Mido Assran, Nicolas Ballas, Wojciech Galuba, Russell Howes, Po-Yao Huang, Shang-Wen Li, Ishan Misra, Michael Rabbat, Vasu Sharma, Gabriel Synnaeve, Hu Xu, Herve Jegou, Julien Mairal, Patrick Labatut, Armand Joulin, and Piotr Bojanowski. DINOv2: Learning robust visual features without supervision. *Transactions on Machine Learning Research*, 2024. 2
- [68] Songyou Peng, Kyle Genova, Chiyu "Max" Jiang, Andrea Tagliasacchi, Marc Pollefeys, and Thomas Funkhouser. Openscene: 3d scene understanding with open vocabularies. In *Proceedings of the IEEE/CVF Conference on Computer Vision and Pattern Recognition (CVPR)*, 2023. 2, 6, 7, 5
- [69] Zhiliang Peng, Wenhui Wang, Li Dong, Yaru Hao, Shaohan Huang, Shuming Ma, and Furu Wei. Kosmos-2: Ground-

- ing multimodal large language models to the world. *arXiv preprint arXiv:2306.14824*, 2023. [2](#), [3](#), [8](#)
- [70] Alec Radford, Jeffrey Wu, Rewon Child, David Luan, Dario Amodei, Ilya Sutskever, et al. Language models are unsupervised multitask learners. *OpenAI blog*, 1(8):9, 2019. [2](#)
- [71] Alec Radford, Jong Wook Kim, Chris Hallacy, Aditya Ramesh, Gabriel Goh, Sandhini Agarwal, Girish Sastry, Amanda Askell, Pamela Mishkin, Jack Clark, Gretchen Krueger, and Ilya Sutskever. Learning transferable visual models from natural language supervision. In *Proceedings of the 38th International Conference on Machine Learning, ICML 2021, 18-24 July 2021, Virtual Event*, pages 8748–8763. PMLR, 2021. [1](#), [2](#), [4](#)
- [72] Santhosh Kumar Ramakrishnan, Aaron Gokaslan, Erik Wijmans, Oleksandr Maksymets, Alexander Clegg, John M Turner, Eric Undersander, Wojciech Galuba, Andrew Westbury, Angel X Chang, et al. Habitat-matterport 3d dataset (hm3d): 1000 large-scale 3d environments for embodied ai. In *Thirty-fifth Conference on Neural Information Processing Systems Datasets and Benchmarks Track (Round 2)*, 2021. [7](#)
- [73] Yongming Rao, Wenliang Zhao, Guangyi Chen, Yansong Tang, Zheng Zhu, Guan Huang, Jie Zhou, and Jiwen Lu. Denseclip: Language-guided dense prediction with context-aware prompting. In *Proceedings of the IEEE/CVF conference on computer vision and pattern recognition*, pages 18082–18091, 2022. [1](#)
- [74] Hanoona Rasheed, Muhammad Maaz, Sahal Shaji, Abdelrahman Shaker, Salman Khan, Hisham Cholakkal, Rao M Anwer, Eric Xing, Ming-Hsuan Yang, and Fahad S Khan. Glamm: Pixel grounding large multimodal model. In *Proceedings of the IEEE/CVF Conference on Computer Vision and Pattern Recognition*, pages 13009–13018, 2024. [3](#)
- [75] Nikhila Ravi, Valentin Gabeur, Yuan-Ting Hu, Ronghang Hu, Chaitanya Ryali, Tengyu Ma, Haitham Khedr, Roman Rädle, Chloe Rolland, Laura Gustafson, et al. Sam 2: Segment anything in images and videos. *arXiv preprint arXiv:2408.00714*, 2024. [2](#), [3](#), [4](#), [8](#)
- [76] Tianhe Ren, Shilong Liu, Ailing Zeng, Jing Lin, Kunchang Li, He Cao, Jiayu Chen, Xinyu Huang, Yukang Chen, Feng Yan, et al. Grounded sam: Assembling open-world models for diverse visual tasks. *arXiv preprint arXiv:2401.14159*, 2024. [3](#), [4](#), [7](#), [8](#), [2](#)
- [77] Robin Rombach, Andreas Blattmann, Dominik Lorenz, Patrick Esser, and Björn Ommer. High-resolution image synthesis with latent diffusion models. In *Proceedings of the IEEE/CVF conference on computer vision and pattern recognition*, pages 10684–10695, 2022. [2](#)
- [78] David Rozenberszki, Or Litany, and Angela Dai. Language-grounded indoor 3d semantic segmentation in the wild. In *European Conference on Computer Vision*, pages 125–141. Springer, 2022. [6](#), [7](#), [8](#), [2](#), [4](#), [5](#)
- [79] Paul K Rubenstein, Chulayuth Asawaroengchai, Duc Dung Nguyen, Ankur Bapna, Zalán Borsos, Félix de Chaumont Quitry, Peter Chen, Dalia El Badawy, Wei Han, Eugene Kharitonov, et al. Audiopalm: A large language model that can speak and listen. *arXiv preprint arXiv:2306.12925*, 2023. [2](#)
- [80] Thomas Schops, Johannes L Schonberger, Silvano Galliani, Torsten Sattler, Konrad Schindler, Marc Pollefeys, and Andreas Geiger. A multi-view stereo benchmark with high-resolution images and multi-camera videos. In *CVPR*, 2017. [8](#)
- [81] Christoph Schuhmann, Romain Beaumont, Richard Vencu, Cade Gordon, Ross Wightman, Mehdi Cherti, Theo Coombes, Aarush Katta, Clayton Mullis, Mitchell Wortsman, et al. Laion-5b: An open large-scale dataset for training next generation image-text models. *Advances in Neural Information Processing Systems*, 35:25278–25294, 2022. [1](#)
- [82] Jonas Schult, Francis Engelmann, Alexander Hermans, Or Litany, Siyu Tang, and Bastian Leibe. Mask3d: Mask transformer for 3d semantic instance segmentation. In *2023 IEEE International Conference on Robotics and Automation (ICRA)*, pages 8216–8223. IEEE, 2023. [2](#), [5](#), [7](#)
- [83] Nur Muhammad Mahi Shafiullah, Chris Paxton, Lerrel Pinto, Soumith Chintala, and Arthur Szlam. Clip-fields: Weakly supervised semantic fields for robotic memory. In *ICRA2023 Workshop on Pretraining for Robotics (PT4R)*, 2023. [1](#)
- [84] Leslie N Smith and Nicholay Topin. Super-convergence: Very fast training of neural networks using large learning rates. In *Artificial intelligence and machine learning for multi-domain operations applications*, pages 369–386. SPIE, 2019. [6](#)
- [85] Jiaming Song, Chenlin Meng, and Stefano Ermon. Denoising diffusion implicit models. In *International Conference on Learning Representations*, 2021. [2](#)
- [86] Yang Song, Jascha Sohl-Dickstein, Diederik P Kingma, Abhishek Kumar, Stefano Ermon, and Ben Poole. Score-based generative modeling through stochastic differential equations. In *International Conference on Learning Representations*, 2021. [2](#)
- [87] Ayça Takmaz, Elisabetta Fedele, Robert W Sumner, Marc Pollefeys, Federico Tombari, and Francis Engelmann. Openmask3d: open-vocabulary 3d instance segmentation. In *Proceedings of the 37th International Conference on Neural Information Processing Systems*, pages 68367–68390, 2023. [2](#), [5](#), [6](#), [7](#)
- [88] Gemini Team, Rohan Anil, Sebastian Borgeaud, Yonghui Wu, Jean-Baptiste Alayrac, Jiahui Yu, Radu Soricut, Johan Schalkwyk, Andrew M Dai, Anja Hauth, et al. Gemini: a family of highly capable multimodal models. *arXiv preprint arXiv:2312.11805*, 2023. [2](#)
- [89] Gemini Team, Petko Georgiev, Ving Ian Lei, Ryan Burnell, Libin Bai, Anmol Gulati, Garrett Tanzer, Damien Vincent, Zhufeng Pan, Shibo Wang, et al. Gemini 1.5: Unlocking multimodal understanding across millions of tokens of context. *arXiv preprint arXiv:2403.05530*, 2024. [2](#)
- [90] Hugo Touvron, Thibaut Lavril, Gautier Izacard, Xavier Martinet, Marie-Anne Lachaux, Timothée Lacroix, Baptiste Rozière, Naman Goyal, Eric Hambro, Faisal Azhar, et al. Llama: Open and efficient foundation language models. *arXiv preprint arXiv:2302.13971*, 2023. [2](#)
- [91] Hugo Touvron, Louis Martin, Kevin Stone, Peter Albert, Amjad Almahairi, Yasmine Babaei, Nikolay Bashlykov, Soumya Batra, Prajjwal Bhargava, Shruti Bhosale, et al.

- Llama 2: Open foundation and fine-tuned chat models. *arXiv preprint arXiv:2307.09288*, 2023. 2
- [92] Johanna Wald, Armen Avetisyan, Nassir Navab, Federico Tombari, and Matthias Nießner. Rio: 3d object instance re-localization in changing indoor environments. In *Proceedings of the IEEE/CVF International Conference on Computer Vision*, pages 7658–7667, 2019. 7
- [93] Peng Wang, An Yang, Rui Men, Junyang Lin, Shuai Bai, Zhikang Li, Jianxin Ma, Chang Zhou, Jingren Zhou, and Hongxia Yang. Ofa: Unifying architectures, tasks, and modalities through a simple sequence-to-sequence learning framework. In *International Conference on Machine Learning*, pages 23318–23340. PMLR, 2022. 3
- [94] Tai Wang, Xiaohan Mao, Chenming Zhu, Runsen Xu, Ruiyuan Lyu, Peisen Li, Xiao Chen, Wenwei Zhang, Kai Chen, Tianfan Xue, Xihui Liu, Cewu Lu, Dahua Lin, and Jiangmiao Pang. EmbodiedScan: A Holistic Multi-Modal 3D Perception Suite Towards Embodied AI, 2023. 2, 8
- [95] Xiaoyang Wu, Zhuotao Tian, Xin Wen, Bohao Peng, Xihui Liu, Kaicheng Yu, and Hengshuang Zhao. Towards large-scale 3d representation learning with multi-dataset point prompt training. *arXiv preprint arXiv:2308.09718*, 2023. 6, 4
- [96] Jiarui Xu, Shalini De Mello, Sifei Liu, Wonmin Byeon, Thomas Breuel, Jan Kautz, and Xiaolong Wang. Groupvit: Semantic segmentation emerges from text supervision. In *Proceedings of the IEEE/CVF Conference on Computer Vision and Pattern Recognition*, pages 18134–18144, 2022. 1
- [97] An Yang, Baosong Yang, Binyuan Hui, Bo Zheng, Bowen Yu, Chang Zhou, Chengpeng Li, Chengyuan Li, Dayiheng Liu, Fei Huang, et al. Qwen2 technical report. *arXiv preprint arXiv:2407.10671*, 2024. 2
- [98] Jihan Yang, Runyu Ding, Weipeng Deng, Zhe Wang, and Xiaojuan Qi. Regionplc: Regional point-language contrastive learning for open-world 3d scene understanding. In *Proceedings of the IEEE/CVF Conference on Computer Vision and Pattern Recognition*, 2024. 2, 3, 5, 6, 7, 8
- [99] Chandan Yeshwanth, Yueh-Cheng Liu, Matthias Nießner, and Angela Dai. Scannet++: A high-fidelity dataset of 3d indoor scenes. In *Proceedings of the IEEE/CVF International Conference on Computer Vision*, pages 12–22, 2023. 1, 2, 4, 6, 7, 5
- [100] Yingda Yin, Yuzheng Liu, Yang Xiao, Daniel Cohen-Or, Jingwei Huang, and Baoquan Chen. Sai3d: Segment any instance in 3d scenes. In *Proceedings of the IEEE/CVF Conference on Computer Vision and Pattern Recognition*, pages 3292–3302, 2024. 5, 7
- [101] Haoxuan You, Haotian Zhang, Zhe Gan, Xianzhi Du, Bowen Zhang, Zirui Wang, Liangliang Cao, Shih-Fu Chang, and Yinfei Yang. Ferret: Refer and ground anything anywhere at any granularity. *arXiv preprint arXiv:2310.07704*, 2023. 2, 3, 8
- [102] Qihang Yu, Ju He, Xueqing Deng, Xiaohui Shen, and Liang-Chieh Chen. Convolutions die hard: open-vocabulary segmentation with single frozen convolutional clip. In *Proceedings of the 37th International Conference on Neural Information Processing Systems*, pages 32215–32234, 2023. 2
- [103] Yuqian Yuan, Wentong Li, Jian Liu, Dongqi Tang, Xinjie Luo, Chi Qin, Lei Zhang, and Jianke Zhu. Osprey: Pixel understanding with visual instruction tuning. In *Proceedings of the IEEE/CVF Conference on Computer Vision and Pattern Recognition*, pages 28202–28211, 2024. 2, 3, 4, 8
- [104] Xiaohua Zhai, Basil Mustafa, Alexander Kolesnikov, and Lucas Beyer. Sigmoid loss for language image pre-training. In *Proceedings of the IEEE/CVF International Conference on Computer Vision*, pages 11975–11986, 2023. 1, 4
- [105] Dong Zhang, Shimin Li, Xin Zhang, Jun Zhan, Pengyu Wang, Yaqian Zhou, and Xipeng Qiu. Speechgpt: Empowering large language models with intrinsic cross-modal conversational abilities. In *The 2023 Conference on Empirical Methods in Natural Language Processing*, 2023. 2
- [106] Youcai Zhang, Xinyu Huang, Jinyu Ma, Zhaoyang Li, Zhaochuan Luo, Yanchun Xie, Yuzhuo Qin, Tong Luo, Yaqian Li, Shilong Liu, et al. Recognize anything: A strong image tagging model. *arXiv preprint arXiv:2306.03514*, 2023. 2
- [107] Jia Zheng, Junfei Zhang, Jing Li, Rui Tang, Shenghua Gao, and Zihan Zhou. Structured3d: A large photo-realistic dataset for structured 3d modeling. In *Computer Vision—ECCV 2020: 16th European Conference, Glasgow, UK, August 23–28, 2020, Proceedings, Part IX 16*, pages 519–535. Springer, 2020. 1, 2, 4, 6, 7, 5
- [108] Xingyi Zhou, Rohit Girdhar, Armand Joulin, Philipp Krähenbühl, and Ishan Misra. Detecting twenty-thousand classes using image-level supervision. In *European Conference on Computer Vision*, pages 350–368. Springer, 2022. 8
- [109] Xueyan Zou, Zi-Yi Dou, Jianwei Yang, Zhe Gan, Linjie Li, Chunyuan Li, Xiyang Dai, Harkirat Behl, Jianfeng Wang, Lu Yuan, et al. Generalized decoding for pixel, image, and language. In *Proceedings of the IEEE/CVF Conference on Computer Vision and Pattern Recognition*, pages 15116–15127, 2023. 2
- [110] Xueyan Zou, Jianwei Yang, Hao Zhang, Feng Li, Linjie Li, Jianfeng Wang, Lijuan Wang, Jianfeng Gao, and Yong Jae Lee. Segment everything everywhere all at once. *Advances in Neural Information Processing Systems*, 36, 2024. 2, 3, 4, 7, 8

Mosaic3D: Foundation Dataset and Model for Open-Vocabulary 3D Segmentation

Supplementary Material

Contents

A Dataset Details	1
A.1 Data Statistics	1
A.2 Data Preprocessing	1
A.3 Pipeline Configurations	2
A.4 Additional Pipeline Experiments	2
B OV3D [48] Implementation Details	2
B.1 Caption Generation	2
B.2 Training Objectives	3
B.3 Results	3
C Experimental Analysis	3
C.1 Model Scaling	3
C.2 Impact of Text Encoders	4
C.3 Annotation-free 3D Referring Segmentation	4
D Additional Results	5
D.1 Quantitative Results	5
D.2 Qualitative Results	5

A. Dataset Details

Below we report the data statistics of our Mosaic3D-5.6M dataset, detail the data preprocessing steps, pipeline configurations used for each dataset in our experiments, and additional data pipeline experiments that utilize 3D instance mask predictions in caption generation process.

A.1. Data Statistics

In Tab. A1, we report the statistics of our generated dataset, including the number of scenes, RGB-D frames, generated captions, and total tokens in captions for each source dataset. Our dataset contains over 30K scenes, and 5.6M captions with a total of 30M tokens across both real and synthetic indoor environments.

Dataset	# Scenes	# Frames	# Captions	# Tokens	Category
ScanNet [24]	1,513	2.5M	1.3M	7.2M	Real
Matterport3D [14]	2,194	0.2M	0.7M	3.8M	Real
ARKitScenes [7]	5,045	4.0M	2.4M	12.6M	Real
ScanNet++ [99]	380	0.2M	0.2M	0.9M	Real
Structured3D [107]	20,065	0.2M	1.0M	5.4M	Synthetic
Total	29,197	7.1M	5.6M	29.9M	

Table A1. **Statistics of our generated dataset.** We report the number of scenes, RGB-D frames, generated captions, and total tokens in captions for each source dataset.

In Tab. A2, we evaluate caption and 3D mask quality across datasets using three metrics. The *unique normalized*

Train dataset	Used ScanNet GT	# Nouns	Mask-Caption Quality Coverage	Entropy	ScanNet20 f-mIoU	ScanNet200 f-mIoU	Head	Com.	Tail
<i>Datasets using only ScanNet as source</i>									
OV3D	✗	2.5K	70.6	72.8	45.6	7.0	18.6	2.1	0.1
RegionPLC	✗	1.4K	77.3	81.0	50.4	8.5	21.1	3.6	0.7
Mosaic3D-SN ²	✗	9.0K	92.6	60.7	65.0	13.0	30.2	6.9	1.4
<i>Datasets using multiple sources</i>									
LEO	✓	2.6K	66.2	-	65.9	14.8	34.3	8.3	1.4
SceneVerse	✓	8.8K	60.0	-	67.3	13.6	32.4	7.3	0.8
EmbodiedScan	✓	0.3K	14.0	-	44.8	6.7	16.1	3.6	0.2
MMScan	✓	6.0K	48.0	-	64.1	11.7	26.1	7.9	0.7
Mosaic3D-5.6M	✗	29.9K	93.7	-	68.1	15.7	32.9	10.8	2.7

Table A2. **Dataset comparison.** We analyze mask-caption quality metrics and annotation-free 3D semantic segmentation performance of different training datasets, while keeping the same model architecture (SpUNet-34C), CLIP model (Recap-CLIP), and loss function (Contrastive).

nouns count measures the total number of unique normalized nouns in captions, with higher count indicating richer and more diverse captions. *Mask coverage (%)* calculates the mean percentage of 3D points with associated captions per scene, where higher coverage enables more effective training. *Mask entropy* (bits) measures mask quality for datasets with partial masks generated from multi-view images (*i.e.* OV3D, RegionPLC, and Mosaic3D-5.6M) without using GT. It calculates Shannon entropy of GT instance ID distributions within each mask—higher entropy indicates that a mask contains multiple GT instances, suggesting less accurate mask boundaries. Mosaic3D-5.6M demonstrates superior caption diversity and mask quality compared to both existing large-scale 3D-text datasets and previous open-vocabulary 3D segmentation datasets, validating its value as a new dataset.

A.2. Data Preprocessing

- **ScanNet [24]** To optimize computational efficiency while maintaining adequate spatial coverage, we process every 20th RGB-D frame from each scene. Prior to processing, we resize all RGB-D frames to 640×480 resolution.
- **ScanNet++ [99]** From the official dataset, we utilize the “*DSLR*” image collection. Following repository guidelines, we generate synthetic depth images using the reconstructed mesh and camera parameters. After correcting for distortion in both RGB and depth images and adjusting camera intrinsics, we process every 10th frame through our annotation pipeline. Point clouds are generated via surface sampling on the reconstructed meshes.
- **ARKitScenes [7]** We leverage the “*3D Object Detection (3DOD)*” subset, utilizing its RGB-D frames and reconstructed meshes. We use every 10th frame at low resolution (256×192), and apply surface point sampling on

²A subset of Mosaic3D-5.6M using only ScanNet as source dataset.

mesh for point clouds.

- **Matterport3D** [14] We use preprocessed RGB-D frames and point clouds provided by the author of Open-Scene [68].
- **Structured3D** [107] We utilize RGB-D frames from both perspective and panoramic camera. We utilize preprocessed point clouds from the *Pointcept* [23] library, which fuses multi-view depth unprojection with voxel downsampling to get point clouds.

A.3. Pipeline Configurations

Our data generation pipeline leverages multiple Visual Foundation Models to automate the data annotation process. Below we detail the configuration of each model in our pipeline.

- **RAM++** [41]: we utilize the official pretrained checkpoint `ram_plus_swin_large_14m` available at <https://huggingface.co/xinyu1205/recognize-anything-plus-model>.
- **Grounded-SAM** [76]: We employ the official checkpoint of Grounding-DINO [59] `IDEA-Research/grounding-dino-tiny` accessed through HuggingFace at <https://huggingface.co/IDEA-Research/grounding-dino-tiny>, together with SAM2 [75] with checkpoint `sam2_hiera_l`, available at <https://huggingface.co/facebook/sam2-hiera-large>. For the postprocessing, we process the output bounding boxes from Grounding-DINO using a box score threshold of 0.25 and a text score threshold of 0.2. We then apply non-maximum suppression (NMS) with an IoU threshold of 0.5 to remove redundancy. To ensure meaningful region proposals, we filter out excessively large boxes that occupy more than 95% of the image area. These refined bounding boxes are then passed to SAM2 for mask prediction.
- **Osprey** [103]: We utilize the official pretrained `sunshine-lwt/Osprey-Chat-7b` checkpoint, available at <https://huggingface.co/sunshine-lwt/Osprey-Chat-7b>. The generation parameters are set with a temperature of 1.0, `top_p` of 1.0, beam search size of 1, and the maximum number of new tokens to 512.

A.4. Additional Pipeline Experiments

We explore two additional data pipeline configurations that use Segment3D [40] masks for segmentation while maintaining Osprey [103] for captioning:

- **Segment3D**: We utilize complete Segment3D masks and obtain captions by aggregating descriptions from multiple projected views of each mask. This approach maintains mask completeness but may result in multiple captions being assigned to a single mask from different viewpoints.

System: A chat between a curious human and an artificial intelligence assistant. The assistant gives helpful, detailed, and polite answers to the human’s questions.

User: `<image>` This provides an overview of the picture. Please give me a short description of `<mask><pos>`, using a short phrase.

Table A3. **Osprey region caption prompt.** Osprey [103] utilizes this prompt along with segmentation masks generated by Grounded-SAM to produce descriptive captions for each region.

- **Segment3D - Mosaic**: We use partial Segment3D masks as seen from individual views and generate captions based on these view-specific projections. While masks are partial, each mask-caption pair is aligned since it represents the exact visible region from a specific viewpoint.

The results in Tab. A4 demonstrate that Segment3D - Mosaic outperforms the baseline Segment3D approach, highlighting the importance of precise mask-text pair alignment. However, both Segment3D variants are outperformed by our Mosaic3D pipeline, which suggests that our combination of RAM++ [41], Grounded-SAM [76], and SEEM [110] provides superior segmentation quality.

Pipeline	ScanNet20 [24]		ScanNet200 [78]	
	f-mIoU	f-mAcc	f-mIoU	f-mAcc
Segment3D [40]	50.6	76.6	8.3	19.1
Segment3D [40] - Mosaic	57.3	79.6	10.6	22.8
Mosaic3D	65.0	82.5	13.0	24.5

Table A4. **Segment3D data pipeline evaluation results.**

B. OV3D [48] Implementation Details

Since there is no publicly available code and data for OV3D [48], we utilized our re-implemented version of OV3D for data visualization (Fig. 2) and statistics (Fig. 4) in the main manuscript. In this section, we provide detailed explanations of our re-implementation results.

B.1. Caption Generation

OV3D [48] obtains entity-level text descriptions of an image through multi-round conversations with LLaVA-1.5 [57]:

1. In the first round, LLaVA-1.5 is prompted to generate an image caption describing the overall scene.
2. In the second round, LLaVA-1.5 is prompted to extract entity names from the generated image caption.
3. In the final round, LLaVA-1.5 is prompted to generate detailed entity descriptions for each extracted entity name.

During our implementation, we encountered inconsistencies in LLaVA-1.5’s response formats. To ensure structured and consistent entity-level text descriptions, we modified the final prompt to request responses in JSON format, as shown in Table A5, while maintaining the original prompts for the first two rounds.

User: Please describe each of the above things that appear in the image with three different nouns or phrases. Format your response as a JSON object with the object names as keys and the list of three nouns or phrases as values. For example: {"entity name A": ["description A1", "description A2", "description A3"], "entity name B": ["description B1", "description B2", "description B3"],...}

Assistant: Here is the dictionary of the concrete objects and background classes in the image:

Table A5. **Modified OV3D entity description prompt.** We modified the original OV3D [48] prompt to request JSON responses for consistent entity descriptions. For brevity, we omit the previous conversation history that is included in the actual prompt.

In addition, our experimental results in Table A7 revealed that LLaVA-1.5’s performance in entity name detection was suboptimal, which significantly impacts OV3D’s overall effectiveness. To overcome this limitation, we introduce OV3D++, an enhanced version that uses RAM++ [41]’s robust tagging capabilities for entity detection while preserving the original entity description process, as shown in Table A6.

B.2. Training Objectives

We experiment with three different training objectives to reproduce OV3D [48]’s performance:

- **DenseAlign:** The original dense alignment loss proposed in OV3D, which maximizes the similarity between text embeddings and point-wise visual features.
- **Align:** A simplified version of dense alignment that computes similarity between text embeddings and pooled visual features within the mask region.
- **Contrastive:** A contrastive learning objective proposed in RegionPLC [98] that pulls matching text-visual pairs closer while pushing non-matching pairs apart in the embedding space.

For fair comparison, we use SparseUNet34C [21] as the backbone network architecture across all experiments, which is the same architecture used in Mosaic3D, and maintain identical training configurations with the only variations being in the training objectives and data generation pipelines.

User: This is a list of entities, including concrete objects and background classes, in the image: <tag>. Based on your description and the given list of entities, please describe each entity with three different nouns or phrases. Format your response as a JSON object with the object names as keys and the list of three nouns or phrases as values. For example: {"entity name A": ["description A1", "description A2", "description A3"], "entity name B": ["description B1", "description B2", "description B3"],...}

Assistant: Here is the dictionary of the concrete objects and background classes in the image:

Table A6. **OV3D++ entity description prompt with tags.** We use RAM++ [41]’s image tagging output results as the placeholder <tag> to leverage its robust entity detection capabilities. For brevity, we omit the previous conversation history that is included in the actual prompt.

B.3. Results

As shown in Table A7, our direct re-implementation (OV3D-rep) is unable to fully reproduce the performance reported in the original OV3D paper [48]. However, our improved version (OV3D++) with RAM++ [41] tagging achieves better results than the original paper in most metrics when using Contrastive loss, except for f-mIoU on ScanNet20 [24]. Notably, Contrastive loss consistently outperforms other loss functions across all settings, which motivates our choice to use Contrastive loss in Mosaic3D as well. While OV3D++ shows significant improvements over the baseline, it is ultimately surpassed by Mosaic3D, demonstrating the effectiveness of Mosaic3D data engine in generating more fine-grained and comprehensive captions.

C. Experimental Analysis

C.1. Model Scaling

Model capacity. Building on the data scaling analysis, we additionally examine how model scales impact performance. We systematically increase the model sizes of 3D encoders while keeping other components fixed. We vary the size of Sparse ConvUNet by changing the model depth and widths following literature [36], where the smallest model, SPUNet14A, has 11.1M trainable parameters, whereas the largest variants, SPUNet101C, has 256M parameters. For these experiments, we fix the training dataset to include ScanNet, ARKitScenes, and ScanNet++. As shown in Fig. A1, increasing model capacity generally leads to better perfor-

Method	Loss	ScanNet20 [24]		ScanNet200 [78]	
		f-mIoU	f-mAcc	f-mIoU	f-mAcc
OV3D [48]	DenseAlign	64.0	76.3	8.7	-
OV3D-rep	DenseAlign	34.7	54.9	4.6	8.3
OV3D-rep	Align	20.0	34.0	2.4	5.4
OV3D-rep	Contrastive	45.6	69.8	6.9	14.3
OV3D++	DenseAlign	54.3	71.6	7.0	12.0
OV3D++	Align	22.5	37.6	3.1	5.6
OV3D++	Contrastive	58.4	76.7	9.2	16.7
Mosaic3D	Contrastive	65.0	82.5	13.0	24.5

Table A7. **Re-implementation and improvement of OV3D [48].** We present our re-implementation results of OV3D with three different training objectives: DenseAlign, Align, and Contrastive. OV3D-rep denotes our re-implementation, while OV3D++ is our improved version using RAM++ [41] tagging.

mance, with diminishing returns after 100M parameters. **Multi-dataset synergistic learning with PPT [95].** Since our Mosaic3D dataset combines multiple datasets with different capture settings and environments, there potentially exists domain gaps between each subset that could hinder effective joint training. Recent work by Wu *et al.* [95] demonstrates that adapting dataset-specific learnable prompts in normalization layers can reduce negative transfer effects when training on multiple point cloud datasets. Building on this insight, we adopt their Point Prompt Training (PPT) approach to enhance our joint training process. As shown in Fig A1, models using PPT demonstrate better scaling compared to standard joint training, confirming PPT’s effectiveness in harmonizing multi-source training on our dataset.

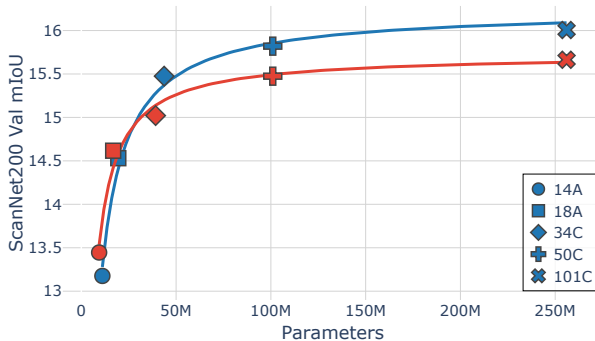


Figure A1. **Model performance scales with model size.** We observe consistent improvements in open-vocabulary semantic segmentation on ScanNet200 [78] as we increase the amount of training data. This shows the value of our large-scale data generation pipeline in improving open-vocabulary 3D scene understanding.

C.2. Impact of Text Encoders

To analyze how different text encoders affect open-vocabulary 3D segmentation performance, we evaluate various CLIP text encoders while keeping the 3D encoder

architecture (SPUNet34C) and other components fixed. Table A8 presents the zero-shot performance on ScanNet20 and ScanNet200 benchmarks. We compare standard CLIP text encoders including CLIP/B32, CLIP/B16, and CLIP/L14@336px [71], as well as recently proposed variants like Recap-CLIP [55] and SigLIP [104].

Among all variants, Recap-CLIP achieves the best overall performance with 68.1% f-mIoU on ScanNet20 and 15.7% f-mIoU on ScanNet200. This represents a +0.3% and +0.9% improvement over the base CLIP/B16 model respectively. The superior performance of Recap-CLIP aligns with its enhanced text-image alignment ability demonstrated in 2D vision tasks. Based on these comprehensive experiments, we select Recap-CLIP as our default text encoder for all subsequent experiments. To ensure fair comparisons with previous work, we maintain consistency by using the same text encoder configuration when reproducing baseline results, as shown in Tables 1, 3, and A7. This standardization enables direct performance comparisons and validates the improvements achieved by our proposed approach.

CLIP Model	ScanNet20 [24]		ScanNet200 [78]	
	f-mIoU	f-mAcc	f-mIoU	f-mAcc
CLIP/B16 [71]	67.1	83.8	14.4	27.7
CLIP/B32 [71]	<u>67.8</u>	<u>84.5</u>	14.8	26.5
CLIP/L14@336px [71]	64.2	81.9	14.9	27.7
SigLIP [104]	66.3	84.6	<u>15.3</u>	29.0
Recap-CLIP [55]	68.1	84.4	15.7	<u>28.3</u>

Table A8. **Impact of CLIP text encoders on open-vocabulary 3D semantic segmentation.** We train our SPUNet34C architecture on the full Mosaic3D-5.6M dataset (5 subsets) with different CLIP text encoders while keeping other components fixed. Recap-CLIP [55] achieves the best overall performance across both ScanNet20 and ScanNet200 benchmarks, demonstrating the importance of text encoder selection for zero-shot generalization.

C.3. Annotation-free 3D Referring Segmentation

To quantitatively analyze the attention between free-form text queries and point features shown in Fig. 7, we leverage the 3D referring segmentation annotations from ScanRefer [15]. This allows us to evaluate how well our model’s attention aligns with human-annotated referring expressions in 3D scenes. Specifically, we evaluate our model’s zero-shot performance on the ScanRefer validation set without any fine-tuning on the 3D referring segmentation task. For each referring expression in ScanRefer, we use it as a text query to obtain attention maps between the query and point features. We then threshold the cosine similarity scores to obtain binary segmentation masks, where points with positive similarity scores (greater than 0) are considered as the predicted region. The predicted masks are compared against ground truth annotations using standard IoU metrics.

As shown in Table A9, our method outperforms both OpenScene-3D [68] and RegionPLC [98], demonstrating its superior ability to highlight relevant regions for free-form text queries. These results demonstrate that our model not only excels at semantic segmentation with simple class names but also achieves superior zero-shot performance on more complex free-form referring expressions, quantitatively validating its effectiveness as a general-purpose 3D vision-language foundation model.

Method	OpenScene-3D [†] [68]	RegionPLC [‡] [98]	Mosaic3D
mIoU	3.1	3.7	5.3

Table A9. **Annotation-free 3D referring segmentation on ScanRefer [15]**. [†] and [‡] denote official checkpoints and our reproductions, respectively.

D. Additional Results

D.1. Quantitative Results

In Tab. A10, We conduct a comprehensive evaluation of our model’s performance across different category frequencies in ScanNet200. Following standard practice [78], we categorize labels into head, common, and tail groups based on their occurrence frequency in the dataset. As shown in Tab. A10, our approach achieves consistent improvements across all category groups compared to previous methods. Notably, we observe the relative gain is more substantial on common and tail categories as we incorporate more training datasets, highlighting the effectiveness of our multi-dataset training strategy in learning robust features across varying scene distributions.

Method	ScanNet200 val mIoU (%)		
	Head	Common	Tail
OpenScene-3D [†]	16.4	2.6	0.2
RegionPLC [‡]	24.2	2.7	0.4
Mosaic3D			
- SN [24]	30.2	6.9	1.4
- SN [24] + AR [7]	32.4	9.3	2.0
- SN [24] + AR [7] + SN2 [99]	33.3	10.0	2.6
- SN [24] + AR [7] + SN2 [99] + M [14]	32.9	10.0	2.5
- SN [24] + AR [7] + SN2 [99] + M [14] + S3D [107]	32.9	10.8	2.7

Table A10. **Category-wise performance analysis on ScanNet200 [78]**. [†] and [‡] denote official checkpoints and our reproductions, respectively.

D.2. Qualitative Results

In Fig. A2, we present additional qualitative visualizations of our generated 3D mask-text pair datasets, where we carefully selected mask-text pairs to effectively demonstrate the diversity and quality of our generated data. Furthermore, in Fig. A3, we showcase attention maps for diverse text

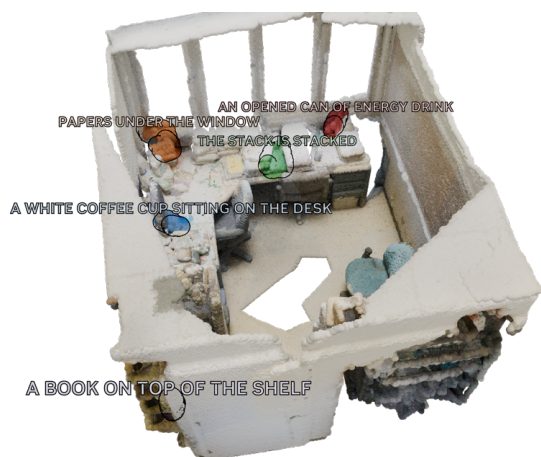
queries across various scenes, which demonstrates that our model can effectively attend to relevant regions in response to different types of queries, ranging from object-centric descriptions to more abstract concepts like affordances. In Fig. A4, we present qualitative results of annotation-free 3D semantic segmentation on ScanNet200 [78]. Our model shows promising results, particularly in the first scene where it demonstrates an interesting behavior - while the ground truth annotates an integrated chair-desk unit entirely as a chair, Mosaic3D distinctly separates and predicts the desk and chair components. This showcases a potential advantage of our annotation-free approach to training 3D foundation models, where the model can learn more nuanced semantic distinctions that might be overlooked in manual annotations.



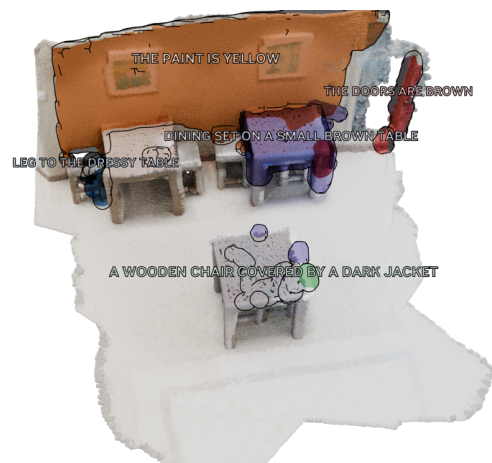
(a) scene0055_02 (ScanNet)



(b) scene0128_00 (ScanNet)



(c) scene0211_01 (ScanNet)



(d) scene0324_00 (ScanNet)



(e) 47333055 (ARKitScenes)



(f) 42898477 (ARKitScenes)

Figure A2. More visualization of the 3D mask-text pairs in our Mosaic3D-5.6M dataset. A subset of mask-text pairs has been chosen for better visualization.

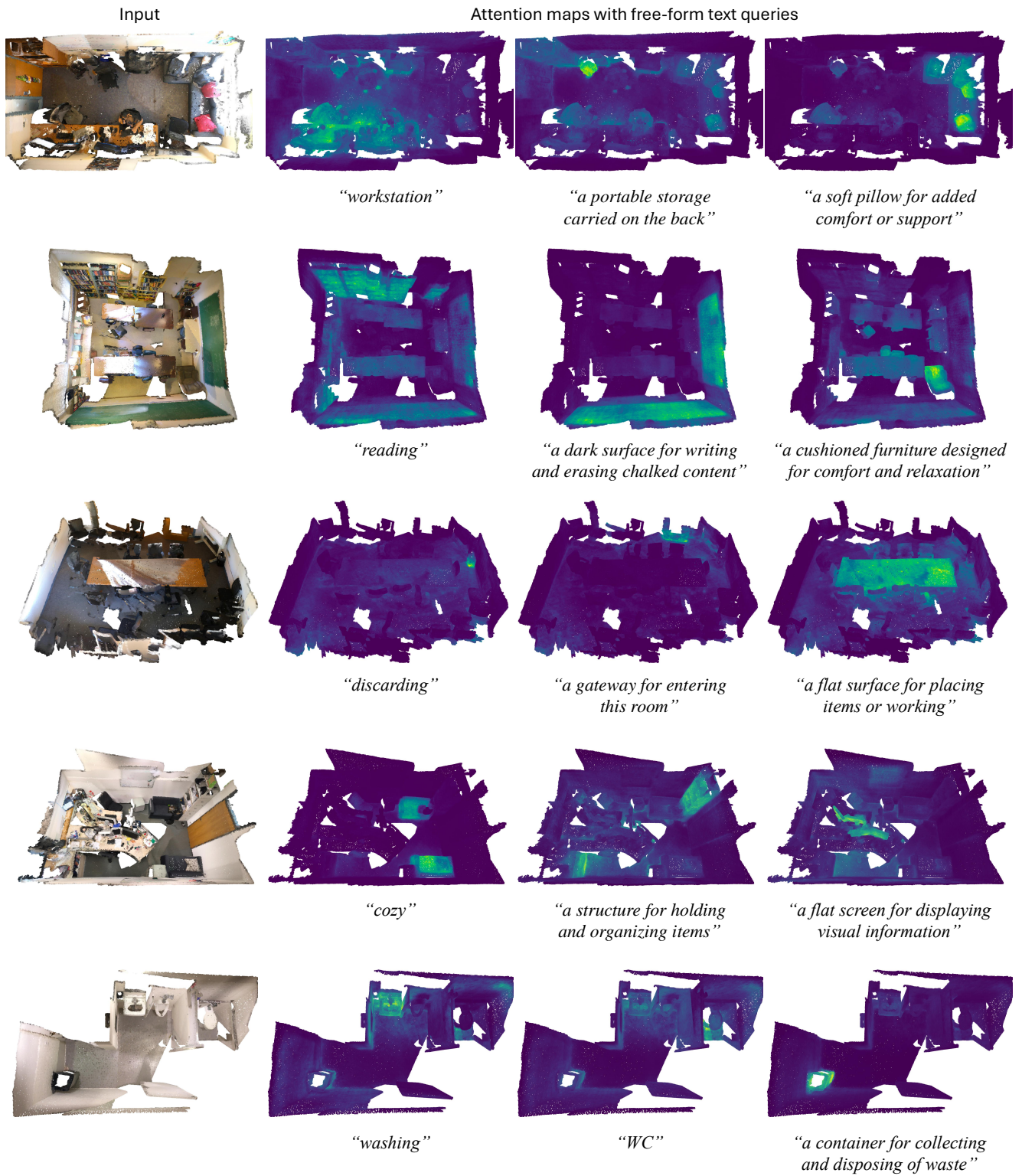


Figure A3. **Attention visualization of Mosaic3D as a 3D foundational model.** We observe that our model can highlight relevant regions even without explicitly mentioning ScanNet [24, 78] class names in queries. The model also effectively attends to regions related to abstract concepts like affordances (e.g., reading, discarding, washing).

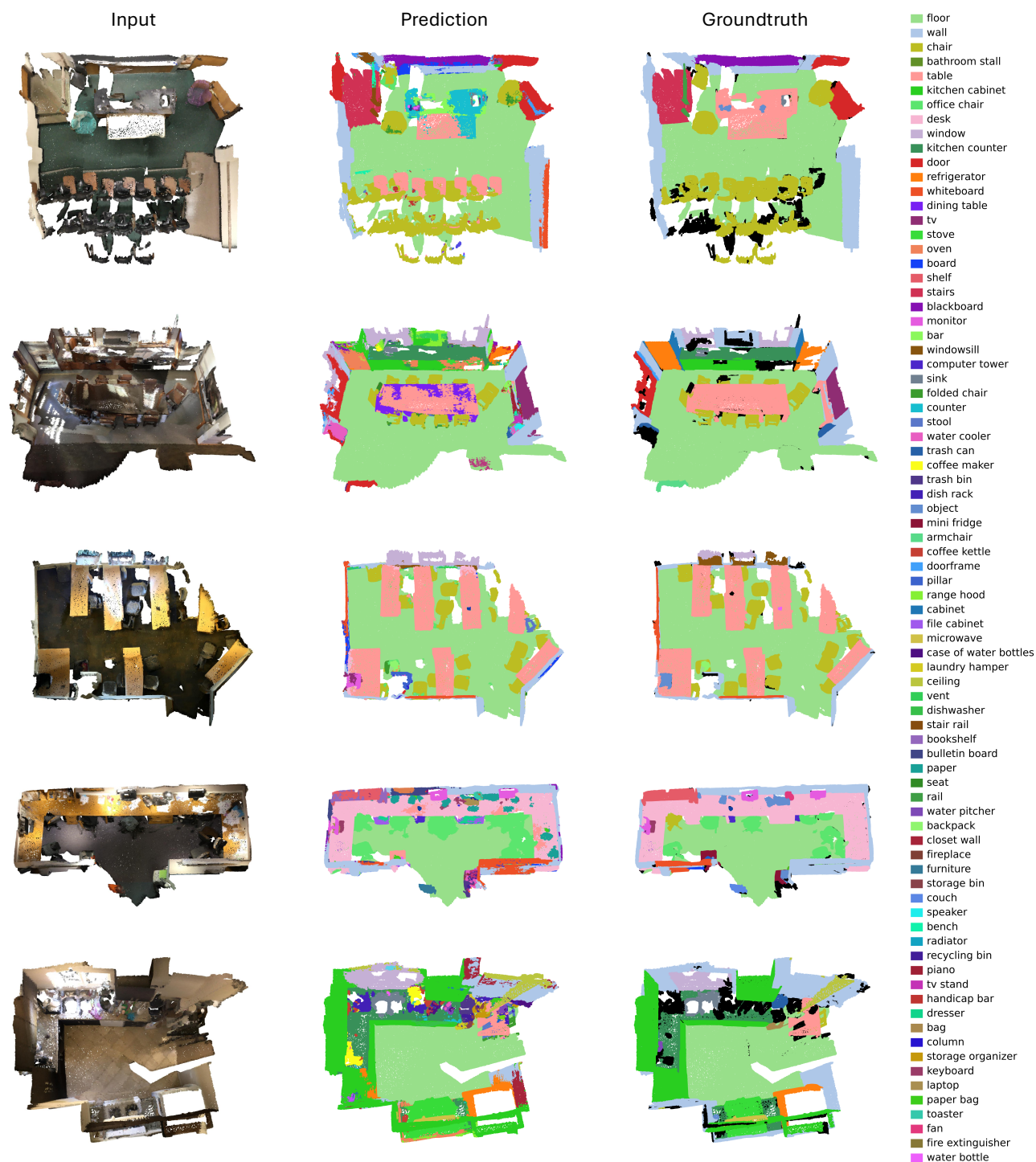


Figure A4. **Qualitative results of annotation-free 3D semantic segmentation on ScanNet200 [78].** Despite being trained without ground truth annotations, Mosaic3D shows competitive results on ScanNet200 [78].